may be implication of communication between mitochondria and membrane-enclosed structures of HCV RC in ATP transport through membrane-to-membrane contact. As indicated in Figure S5, putative sites of the viral RNA replication with high Venus/CFP ratios were mainly localized proximal to mitochondria. Studies are ongoing to understand the mechanism(s) underlying this phenomenon, as well as to determine if changes in ATP levels at intracellular sites supporting replication might also be observed for other RNA or DNA viruses.

In summary, we have used a FRET-based ATP indicator called ATeam to monitor ATP levels in living cells where viral RNA replicates by designing HCV replicons harboring wild-type or mutated ATeam probes inserted into the C-terminal domain of NS5A. We evaluated changes in ATP levels during HCV RNA replication and demonstrated elevated ATP levels at putative sites of replication following detection of FRET signals, which appeared as dot-like foci within the cytoplasm. The ATeam system may become a powerful tool in microbiology research by enabling determination of subcellular ATP localization in living cells infected or associated with microbes, as well as investigation of the regulation of ATP-dependent processes during the lifecycle of various pathogens.

Materials and Methods

Chemicals

PSI-6130 (β-$_D$-2′-Deoxy-2′-fluoro-2′-*C*-methylcytidine) and recombinant human IFN-alpha2b were obtained from Pharmasset Inc. (Princeton, NJ) [23,24] and Schering-Plough (Kenilworth, NJ), respectively. OliA and 2DG were purchased from Sigma-Aldrich (St. Louis, MO). ATP used in this study was complexed with equimolar concentrations of magnesium chloride before use in the experiments.

Plasmids

The construction of the ATeam plasmids pRSET-AT1.03, pRSET-AT1.03^{YEMK} and pRSET-AT1.03$^{R122K/R126K}$, which express wild-type ATeam (AT1.03), as well as a high-affinity mutant (AT1.03^{YEMK}) and a non-binding mutant (AT1.03^{RK}), has been previously described [2]. pHH/SGR-Luc (also termed SGR/luc) contains cDNA of a subgenomic replicon of HCV JFH-1 isolate (genotype 2a; [14]) with firefly luciferase flanked by the Pol I promoter and the Pol I terminator, yielding efficient RNA replication upon DNA transfection [26]. pHH/SGR-Luc/GND (also termed SGR/luc-GND), in which a point mutation of the GDD motif of the NS5B was introduced in order to abolish RNA-dependent RNA polymerase activity, was used as a negative control. pHH/SGR (also termed SGR) was created by deleting the luciferase gene in pHH/SGR-Luc. To generate a series of SGR-ATeam plasmids, wild-type or mutant ATeam genes were inserted into pHH/SGR-Luc or pHH/SGR at the Xho I site of NS5A (between amino acids 418 and 419) [25]. The ATeam genes were also inserted into the same site of pCAGNS5A, which contains the NS5A gene of JFH-1 downstream of the CAG promoter and hemagglutinin (HA) tag [26], yielding NS5A-ATeam plasmids. To generate a plasmid expressing NS3-NS5B-AT1.03 under the control of the CAG promoter, a DNA fragment containing the coding region of NS3/NS4A/NS4B/NS5A-AT1.03/NS5B of SGR/luc-ATeam was inserted into the pCAGGS vector [40]. Exact cloning strategies are available upon request.

Cell culture and plasmid transfection

Human hepatoma Huh-7 cells were propagated in Dulbecco's modified Eagle's medium (DMEM) supplemented with 10% fetal calf serum (FCS) as well as minimal essential medium non-essential amino acid (MEM NEAA)(Invitrogen, Carlsbad, CA) in the presence of 100 units/ml of penicillin and 100 μg/ml of streptomycin. The Huh-7-derived cell lines JFH-1/4-1 and JFH-1/4-5, which support replication of SGR RNA of HCV JFH-1 (genotype 2a) and NK5.1/0-9, which carries the SGR RNA of Con1 NK5.1 (genotype 1b), were cultured and maintained under previously described conditions [15]. DNA transfection was performed using a TransIT-LT1 transfection reagent (Takara, Shiga, Japan) in accordance with the manufacturer's instructions.

CE-TOF MS analysis

Huh-7 cells were mock-infected or infected with HCVcc derived from a wild-type JFH-1 isolate at a multiplicity of infection of 1. When most cells had become virus positive, as confirmed by immunofluorescence, with no observable cell damage at 9 days post-infection, equal amounts of cells with and without HCV infection were scraped with MeOH including 10 μM of an internal standard after washing twice with 5% mannitol solution. Replicon cells (JFH-1/4-5) that were cultured in the absence of G418 for 2 days were harvested and prepared as above. The extracts were mixed with chloroform and water, followed by centrifugation at 2,300× *g* for 5 min at 4°C, The upper aqueous layer was centrifugally filtered through a 5-kDa cutoff filter to remove proteins. The filtrate was lyophilized and dissolved in water, then subjected to CE-TOF MS analysis. CE-TOF MS experiments were performed using an Agilent CE-TOF MS system (Agilent Technologies, Waldbronn, Germany) as described previously [41].

ATP consumption assay

The ATP consumption assay using permeabilized replicon cells was carried out as previously described [13,22] with slight modifications, so that it was unnecessary to add either exogenous phosphocreatine or creatine phosphokinase to minimize ATP reproduction in cells. Cells (2×10^6) cultured in the presence or absence of PSI-6130 for 72 h were treated with 5 μg Actinomycin D/ml, followed by trypsinization and 3 washes with cold buffer B (20 mM HEPES-KOH [pH 7.7], 110 mM potassium acetate, 2 mM magnesium acetate, 1 mM EGTA, and 2 mM dithiothreitol). The cells were permeabilized by incubation with buffer B containing 50 μg/ml digitonin for 5 min on ice and the reaction was stopped by washing 3 times with cold buffer B. The permeabilized cells (1×10^5) were resuspended with 100 μl buffer B containing 5 μM ATP, GTP, CTP, and UTP, 20 μM $MgCl_2$, and 5 μg/ml Actinomycin D. After incubation at 27°C for 15 min, samples were centrifuged, and 20 μl of the supernatant was then mixed with 5 μl of 5× passive lysis buffer (Promega, Madison, WI). The ATP level was determined using a CellTiter-Glo Luminescent cell viability assay system (Promega). All assays were performed at least in triplicate.

Live cell microscopy

Plasmids carrying the ATP indicators were transfected at 48 h (ATeam and NS5A-ATeam) or 4 days (SGR-ATeam) before imaging of the cells. One day before imaging, the cells were seeded onto 30-mm glass-bottomed dishes (AGC Techno Glass, Chiba, Japan) at about 60% confluency. For imaging, the cells were maintained in phenol red-free DMEM containing 20 mM HEPES-KOH [pH 7.7], 10% FCS and MEM NEAA.

Two kinds of confocal microscopies were used to perform the FRET analysis in this study as follows. Since the ways of acquisition of each spectrum were quite different between the two microscopies, differences in the values of the Venus/CFP ratios in different

experiments were observed. In Figures 2, 4B and S2, cells were imaged using a confocal inverted microscope FV1000 (Olympus, Tokyo, Japan) equipped with an oil-immersion 60× Olympus UPlanSApo objective (NA = 1.35). Cells were maintained on the microscope at 37°C with a stage-top incubation system (Tokai Hit, Shizuoka, Japan). Cells were excited by a 405-nm laser diode, and CFP and Venus were detected at 480–500 nm and 515–615 nm wavelength ranges, respectively. In the analysis shown in Figures 5, 6, S3, S4 and S5, FRET images were obtained using a Zeiss LSM510 Meta confocal microscope with an oil-immersion 63× Zeiss Plan-APOCHROMAT objective (NA = 1.4)(Carl Zeiss, Jena, Germany). Cells were maintained on the microscope at 37°C with a continuous supply of a 95% air and 5% CO_2 mixture using a XL-3 incubator (Carl Zeiss). Cells were excited by a 405-nm blue diode laser, and emission spectra of 433–604 nm wavelength range were obtained using an equipped scanning module (META detector) [42,43]. Images were computationally processed by a linear unmixing algorithm using the reference spectrum of CFP and Venus, which were obtained from individual fluorescence-expressing cells. All image analyses were performed using MetaMorph (Molecular Devices, Sunnyvale, CA). Fluorescence intensities of cytoplasmic areas in NS5A-ATeam transfected cells were calculated by subtraction of the signal intensities of the nucleus from the signal intensities of the whole cell, which was standardized by the area of the corresponding cytoplasmic region. Fluorescence intensities of cytoplasmic areas and at dot-like structures corresponding to the putative viral replicating sites in SGR-ATeam-transfected cells were measured and calculated as follows. All pixels above CFP intensity levels of 100–200 were selected. The positions of dot-like structures were then determined by examining areas greater than 0.5×10^{-12} square meters and the intensity of each dot was measured. The fluorescence intensity of the cytoplasmic area, excluding that of the putative viral replicating sites in each cell, was calculated by subtraction of the signal intensities of the nucleus and the dot-like structures, as determined above, from the signal intensity of the whole cell, which was standardized by the area of the corresponding cytoplasmic region. Each Venus/CFP emission ratio was calculated by dividing pixel-by-pixel a Venus image with a CFP image.

To investigate the relationship between Venus/CFP ratios and ATP concentrations in cells, calibration procedures were performed according to previous reports [29,30]. Huh-7 cells were transfected with NS5A-AT1.03 or NS5A-AT1.03^{YEMK}. Forty-eight hours later, the cells were permeabilized by incubation with buffer B containing 50 μg/ml digitonin for 5 min at room temperature. The reaction was stopped by washing 3 times with buffer B, followed by the addition of known concentrations of ATP in warmed medium for imaging. FRET analysis, with calibration of the signal intensity in the cytoplasm of each cell, was performed as described above. Plots were fitted with Hill equations with a fixed Hill coefficient of 2; $R = (R_{max}-R_{min})\times[ATP]^2/([ATP]^2+Kd^2)+R_{min}$, where R_{max} and R_{min} are the maximum and minimum fluorescence ratios, respectively and Kd is the apparent dissociation constant.

To analyze the effect of an inhibitor against HCV NS5B polymerase, the medium for the cells replicating SGR-ATeam was changed to medium containing various concentrations of PSI-6130. After 10-min incubation at 37°C under a continuous supply of 95% air and 5% CO_2, fluorescence intensities of cytoplasmic areas and at dot-like structures were determined as described above. Medium containing 0.01% DMSO was used as a negative control.

To visualize mitochondria, MitoTracker Red CMXRos (Molecular Probes, Eugene, OR) was added to the culture medium to a final concentration of 100 nM, incubated for 15 min at 37°C and the cells were then washed twice with phosphate buffered saline (PBS) before FRET analysis of living cells. Images were computationally processed as described above. The reference spectrum of MitoTracker Red CMXRos was obtained from stained parental, non-transfected, Huh-7 cells.

Indirect immunofluorescence

Cells expressing SGR-ATeam were cultured in 30-mm glass-bottomed dishes with an address grid on the coverslip (AGC Techno Glass). After FRET analysis of living cells as described above, the cells were fixed with 4% paraformaldehyde at room temperature for 30 min. After washing with PBS, the cells were permeabilized with PBS containing 0.3% Triton X-100 and individually stained with a rabbit polyclonal antibody against NS3 [44], an anti-NS5A antibody [45], or a mouse monoclonal antibody against dsRNA antibody (Biocenter Ltd., Szirak, Hungary) [46]. The fluorescent secondary antibody used was Alexa Fluor 555-conjugated anti-rabbit- or anti-mouse IgG (Invitrogen). The cells were imaged using a Zeiss LSM510 Meta confocal microscope with an oil-immersion 63× Zeiss Plan-APOCHROMAT objective (NA = 1.4). For dual-color imaging, the ATeam signal was excited with the 488-nm laser line of an argon laser and Alexa Fluor 555 was excited with a 543-nm HeNe laser under MultiTrack mode. Emission filters with a 505- to 530-nm band-pass and 560-nm-long pass filter were used.

Luciferase assay

Huh-7 cells transfected with SGR/luc or SGR/luc-ATeam were harvested at different time points after transfection (Figure 4D) or at 3 days after treatment with PSI-6130 (Figure S6) and lysed in passive lysis buffer (Promega). To monitor HCV RNA replication, the luciferase activity in cells was determined using a Luciferase Assay system (Promega). All assays were performed at least in triplicate.

MTT assay

Cell viability was assessed using the Cell Proliferation Kit II (Roche, Indianapolis, IN) according to the manufacturer's instructions. The kit measures mitochondrial dehydrogenase activity, which is used as a marker of viable cells, using a colorimetric sodium3′-[1(-phenylaminocarbonyl)-3,4-tetrazolium]-bis(4-methoxy-6-nitro)benzene sulfonic acid hydrate (MTT) assay.

Quantification of HCV RNA

HCV RNA copies in the replicon cells with or without PSI-6130 treatment were determined using the real-time detection reverse transcription polymerase chain reaction (RTD-PCR) described previously [47] with the ABI Prisom 7700 sequence detector system (Applied Biosystems Japan, Tokyo, Japan).

Western blotting

The proteins were transferred onto a polyvinylidene difluoride membrane (Immobilon; Millipore, Bedford, MA) after separation by SDS-PAGE. After blocking, the membranes were probed with a rabbit polyclonal anti-NS5A antibody [44], a rabbit polyclonal anti-NS5B antibody (Chemicon, Temecula, CA), or a mouse polyclonal anti-beta-actin antibody (Sigma-Aldrich), followed by incubation with a peroxidase-conjugated secondary antibody and visualization with an ECL Plus Western blotting detection system (GE Healthcare, Buckinghamshire, UK).

Supporting Information

Figure S1 ATP Levels in HCV replicon cells and parental Huh-7 cells determined by CE-TOF MS. ATP metabolites in Huh-7 cells and JFH-1/4-5 cells were measured by

CE-TOFMS. The values of each measurement are shown at left. The right graph shows means with SD of the data at left. Open bar; Huh-7 cells, gray bar; JFH-1/4-5 cells.
(TIF)

Figure S2 Cytoplasmic ATP levels in HCV replicon cells and IFN-treated cells. (Left) The HCV replicon cells JFH-1/4-1, JFH-1/4-5 (genotype 2a) and NK5.1/0-9 (genotype 1b), and parental Huh-7 cells were cultured for 72 h in the absence or presence of 1,000 IU/ml IFN-alpha. Forty-eight hours after transfection with AT1.03, the Venus/CFP emission ratio of each cell was calculated from fluorescent images acquired with the confocal microscope FV1000. All data are presented as means and SD for at least 10 independent cells. (Right) HCV RNA titers in cells corresponding to the left panel were determined using real-time quantitative RT-PCR. Data are presented as means and SD for three independent samples. NTD indicates not detected.
(TIF)

Figure S3 Increase in ATP-enriched dot-like structures in cells replicating SGR-ATeam. Huh-7 cells were transfected with SGR-AT1.03, and analyzed in the same way as described in the legends for Figures 5A and 5B. The lower four panels are five-fold magnifications of the boxed areas in independent cells. Scale bars, 40 μm.
(TIF)

Figure S4 Visualization of the ATP level in cells expressing replication-defective HCV polyprotein. (A) A schematic representation of the NS3-NS5B-AT1.03 plasmid is shown. The HCV polyprotein is indicated by the open boxes. The ATeam gene was inserted into the same site as that for NS5A-ATeam and SGR-ATeam insertion as indicated in the legend for Figure 4A. CAG, CAG promoter. (B) Cells transfected with constructs encoding NS5A, NS5A-AT1.03, NS3-NS5B-AT1.03, SGR or SGR-AT1.03 were analyzed by immunoblotting with anti-NS5A, anti-NS5B or anti-beta-actin antibodies. (C) Huh-7 cells were transfected with NS3-NS5B-AT1.03, and analyzed in the same way as described in the legends for Figures 5A and 5B. The upper panel (Fluorescence) demonstrates signal intensity from a spectral channel with maximum intensity and represents the expression pattern of NS5A-ATeam processed from NS3-NS5B-AT1.03. The lower panels (Venus/CFP ratio) indicate the FRET ratio and a five-fold magnification of the boxed area. Scale bar, 20 μm.
(TIF)

Figure S5 Relationship between ATP-enriched dot-like structures and mitochondria. Huh-7 cells replicating SGR-AT1.03 (right panels) and parental cells (left panel) were analyzed. Active mitochondria were labeled with MitoTracker Red CMXRos in living cells, and were analyzed in the same way as described in the legends for Figures 5A and 5B, using a reference for the MitoTracker spectrum. The lowest panels of SGR-ATeam cells indicate five-fold magnifications of the boxed areas. Scale bars, 20 μm.
(TIF)

Figure S6 Inhibitory effect of PSI-6130 on HCV RNA replication. (A) Replication levels of SGR/luc-AT1.03 RNA in transfected cells were determined by luciferase assay 3 days after treatment with PSI-6130 at the indicated concentrations (μM). The values shown were normalized for transfection efficiency with luciferase activity determined 24 h post-transfection. All data are presented as means and SD for three independent samples. (B) Cell viability was assessed using the MTT assay.
(TIF)

Acknowledgments

We are grateful to Minoru Tobiume, Tadaki Suzuki, Teruyuki Nagamune, Satoshi Yamaguchi, Yoshiharu Matsuura, Hiroto Kambara, Tomoko Date, Su Su Hmwe, Koichi Watashi, Takahiro Masaki and Takanobu Kato for their excellent technical assistance and advice, as well as to Takeharu Nagai for providing the mVenus expression vector and to Atsushi Miyawaki for providing the mseCFP expression vector. We thank our coworkers for their helpful discussions. We also thank Mami Sasaki for her technical assistance and Tomoko Mizoguchi for her secretarial work. We also thank the University of Tokyo Center for NanoBio Integration and the Department of Pathology in the National Institute of Infectious Diseases, Japan, for use of their confocal microscope.

Author Contributions

Conceived and designed the experiments: T. Ando, H. Imamura, T. Wakita, T. Suzuki. Performed the experiments: T. Ando, H. Aizaki. Analyzed the data: T. Ando, H. Imamura, T. Watanabe, T. Wakita, T. Suzuki. Contributed reagents/materials/analysis tools: H. Imamura, R. Suzuki, H. Aizaki. Wrote the paper: T. Ando, T. Suzuki.

References

1. Ranji A, Boris-Lawrie K (2010) RNA helicases: Emerging roles in viral replication and the host innate response. RNA Biol 7: 775–787.
2. Imamura H, Nhat KP, Togawa H, Saito K, Iino R, et al. (2009) Visualization of ATP levels inside single living cells with fluorescence resonance energy transfer-based genetically encoded indicators. Proc Natl Acad Sci U S A 106: 15651–15656.
3. Kato-Yamada Y, Yoshida M (2003) Isolated epsilon subunit of thermophilic F1-ATPase binds ATP. J Biol Chem 278: 36013–36016.
4. Iino R, Murakami T, Iizuka S, Kato-Yamada Y, Suzuki T, et al. (2005) Real-time monitoring of conformational dynamics of the epsilon subunit in F1-ATPase. J Biol Chem 280: 40130–40134.
5. Yagi H, Kajiwara N, Tanaka H, Tsukihara T, Kato-Yamada Y, et al. (2007) Structures of the thermophilic F1-ATPase epsilon subunit suggesting ATP-regulated arm motion of its C-terminal domain in F1. Proc Natl Acad Sci U S A 104: 11233–11238.
6. Bartenschlager R, Sparacio S (2007) Hepatitis C virus molecular clones and their replication capacity in vivo and in cell culture. Virus Res 127: 195–207.
7. Pezacki JP, Singaravelu R, Lyn RK (2010) Host-virus interactions during hepatitis C virus infection: a complex and dynamic molecular biosystem. Mol Biosyst 6: 1131–1142.
8. Suzuki T, Ishii K, Aizaki H, Wakita T (2007) Hepatitis C viral life cycle. Adv Drug Deliv Rev 59: 1200–1212.
9. Cai Z, Liang TJ, Luo G (2004) Effects of Mutations of the Initiation Nucleotides on Hepatitis C Virus RNA Replication in the Cell. J Virol 78: 3633–3643.
10. Moradpour D, Penin F, Rice CM (2007) Replication of hepatitis C virus. Nat Rev Microbiol 5: 453–463.
11. Dumont S, Cheng W, Serebrov V, Beran RK, Tinoco I, Jr., et al. (2006) RNA translocation and unwinding mechanism of HCV NS3 helicase and its coordination by ATP. Nature 439: 105–108.
12. Frick DN (2007) The hepatitis C virus NS3 protein: a model RNA helicase and potential drug target. Curr Issues Mol Biol 9: 1–20.
13. Miyanari Y, Hijikata M, Yamaji M, Hosaka M, Takahashi H, et al. (2003) Hepatitis C virus non-structural proteins in the probable membranous compartment function in viral genome replication. J Biol Chem 278: 50301–50308.
14. Wakita T, Pietschmann T, Kato T, Date T, Miyamoto M, et al. (2005) Production of infectious hepatitis C virus in tissue culture from a cloned viral genome. Nat Med 11: 791–796.
15. Miyamoto M, Kato T, Date T, Mizokami M, Wakita T (2006) Comparison between subgenomic replicons of hepatitis C virus genotypes 2a (JFH-1) and 1b (Con1 NK5.1). Intervirology 49: 37–43.
16. Mankouri J, Tedbury PR, Gretton S, Hughes ME, Griffin SD, et al. (2010) Enhanced hepatitis C virus genome replication and lipid accumulation mediated by inhibition of AMP-activated protein kinase. Proc Natl Acad Sci U S A 107: 11549–11554.
17. Nakashima K, Takeuchi K, Chihara K, Hotta H, Sada K (2011) Inhibition of hepatitis C virus replication through adenosine monophosphate-activated protein kinase-dependent and -independent pathways. Microbiol Immunol 55: 774–782.

18. Nagai T, Ibata K, Park ES, Kubota M, Mikoshiba K, et al. (2002) A variant of yellow fluorescent protein with fast and efficient maturation for cell-biological applications. Nat Biotechnol 20: 87–90.
19. Appleby TC, Anderson R, Fedorova O, Pyle AM, Wang R, et al. (2011) Visualizing ATP-dependent RNA translocation by the NS3 helicase from HCV. J Mol Biol 405: 1139–1153.
20. Cheng W, Arunajadai SG, Moffitt JR, Tinoco I, Jr., Bustamante C (2011) Single-base pair unwinding and asynchronous RNA release by the hepatitis C virus NS3 helicase. Science 333: 1746–1749.
21. Beran RK, Lindenbach BD, Pyle AM (2009) The NS4A protein of hepatitis C virus promotes RNA-coupled ATP hydrolysis by the NS3 helicase. J Virol 83: 3268–3275.
22. Hara H, Aizaki H, Matsuda M, Shinkai-Ouchi F, Inoue Y, et al. (2009) Involvement of creatine kinase B in hepatitis C virus genome replication through interaction with the viral NS4A protein. J Virol 83: 5137–5147.
23. Ma H, Jiang WR, Robledo N, Leveque V, Ali S, et al. (2007) Characterization of the metabolic activation of hepatitis C virus nucleoside inhibitor beta-D-2′-Deoxy-2′-fluoro-2′-C-methylcytidine (PSI-6130) and identification of a novel active 5′-triphosphate species. J Biol Chem 282: 29812–29820.
24. Murakami E, Bao H, Ramesh M, McBrayer TR, Whitaker T, et al. (2007) Mechanism of activation of beta-D-2′-deoxy-2′-fluoro-2′-c-methylcytidine and inhibition of hepatitis C virus NS5B RNA polymerase. Antimicrob Agents Chemother 51: 503–509.
25. Moradpour D, Evans MJ, Gosert R, Yuan Z, Blum HE, et al. (2004) Insertion of green fluorescent protein into nonstructural protein 5A allows direct visualization of functional hepatitis C virus replication complexes. J Virol 78: 7400–7409.
26. Masaki T, Suzuki R, Saeed M, Mori K, Matsuda M, et al. (2010) Production of infectious hepatitis C virus by using RNA polymerase I-mediated transcription. J Virol 84: 5824–5835.
27. Shi ST, Lee KJ, Aizaki H, Hwang SB, Lai MMC (2003) Hepatitis C Virus RNA Replication Occurs on a Detergent-Resistant Membrane That Cofractionates with Caveolin-2. J Virol 77: 4160–4168.
28. Gosert R, Egger D, Lohmann V, Bartenschlager R, Blum HE, et al. (2003) Identification of the Hepatitis C Virus RNA Replication Complex in Huh-7 Cells Harboring Subgenomic Replicons. J Virol 77: 5487–5492.
29. Palmer AE, Jin C, Reed JC, Tsien RY (2004) Bcl-2-mediated alterations in endoplasmic reticulum Ca2+ analyzed with an improved genetically encoded fluorescent sensor. Proc Natl Acad Sci U S A 101: 17404–17409.
30. Dittmer PJ, Miranda JG, Gorski JA, Palmer AE (2009) Genetically encoded sensors to elucidate spatial distribution of cellular zinc. J Biol Chem 284: 16289–16297.
31. Nomaguchi M, Ackermann M, Yon C, You S, Padmanbhan R (2003) De Novo Synthesis of Negative-Strand RNA by Dengue Virus RNA-Dependent RNA Polymerase In Vitro: Nucleotide, Primer, and Template Parameters. J Virol 77: 8831–8842.
32. Klumpp K, Ford MJ, Ruigrok RW (1998) Variation in ATP requirement during influenza virus transcription. J Gen Virol 79(Pt 5): 1033–1045.
33. Vreede FT, Gifford H, Brownlee GG (2008) Role of initiating nucleoside triphosphate concentrations in the regulation of influenza virus replication and transcription. J Virol 82: 6902–6910.
34. Frick DN, Lam AM (2006) Understanding helicases as a means of virus control. Curr Pharm Des 12: 1315–1338.
35. Gurer C, Hoglund A, Hoglund S, Luban J (2005) ATPgammaS disrupts human immunodeficiency virus type 1 virion core integrity. J Virol 79: 5557–5567.
36. Li PP, Itoh N, Watanabe M, Shi Y, Liu P, et al. (2009) Association of simian virus 40 vp1 with 70-kilodalton heat shock proteins and viral tumor antigens. J Virol 83: 37–46.
37. Dennis PB, Jaeschke A, Saitoh M, Fowler B, Kozma SC, et al. (2001) Mammalian TOR: a homeostatic ATP sensor. Science 294: 1102–1105.
38. Zamaraeva MV, Sabirov RZ, Maeno E, Ando-Akatsuka Y, Bessonova SV, et al. (2005) Cells die with increased cytosolic ATP during apoptosis: a bioluminescence study with intracellular luciferase. Cell Death Differ 12: 1390–1397.
39. Berg J, Hung YP, Yellen G (2009) A genetically encoded fluorescent reporter of ATP:ADP ratio. Nat Methods 6: 161–166.
40. Niwa H, Yamamura K, Miyazaki J (1991) Efficient selection for high-expression transfectants with a novel eukaryotic vector. Gene 108: 193–199.
41. Soga T, Ohashi Y, Ueno Y, Naraoka H, Tomita M, et al. (2003) Quantitative metabolome analysis using capillary electrophoresis mass spectrometry. J Proteome Res 2: 488–494.
42. Haraguchi T, Shimi T, Koujin T, Hashiguchi N, Hiraoka Y (2002) Spectral imaging fluorescence microscopy. Genes Cells 7: 881–887.
43. Ishii M, Ikushima M, Kurachi Y (2005) In vivo interaction between RGS4 and calmodulin visualized with FRET techniques: possible involvement of lipid raft. Biochem Biophys Res Commun 338: 839–846.
44. Murakami K, Kimura T, Osaki M, Ishii K, Miyamura T, et al. (2008) Virological characterization of the hepatitis C virus JFH-1 strain in lymphocytic cell lines. J Gen Virol 89: 1587–1592.
45. Inoue Y, Aizaki H, Hara H, Matsuda M, Ando T, et al. (2011) Chaperonin TRiC/CCT participates in replication of hepatitis C virus genome via interaction with the viral NS5B protein. Virology 410: 38–47.
46. Taguwa S, Kambara H, Omori H, Tani H, Abe T, et al. (2009) Cochaperone activity of human butyrate-induced transcript 1 facilitates hepatitis C virus replication through an Hsp90-dependent pathway. J Virol 83: 10427–10436.
47. Takeuchi T, Katsume A, Tanaka T, Abe A, Inoue K, et al. (1999) Real-time detection system for quantification of hepatitis C virus genome. Gastroenterology 116: 636–642.

Virology ∎ (∎∎∎∎) ∎∎∎–∎∎∎

Contents lists available at SciVerse ScienceDirect

Virology

journal homepage: www.elsevier.com/locate/yviro

Trans-complemented hepatitis C virus particles as a versatile tool for study of virus assembly and infection

Ryosuke Suzuki [a,*], Kenji Saito [a], Takanobu Kato [a], Masayuki Shirakura [b], Daisuke Akazawa [a], Koji Ishii [a], Hideki Aizaki [a], Yumi Kanegae [c], Yoshiharu Matsuura [d], Izumu Saito [c], Takaji Wakita [a], Tetsuro Suzuki [e,**]

[a] *Department of Virology II, National Institute of Infectious Diseases, 1-23-1 Toyama, Shinjuku-ku, Tokyo 162-8640, Japan*
[b] *Influenza Virus Research Center, National Institute of Infectious Diseases, Tokyo 208-0011, Japan*
[c] *Institute of Medical Science, University of Tokyo, Tokyo 108-8639, Japan*
[d] *Research Institute for Microbial Diseases, Osaka University, Osaka 565-0871, Japan*
[e] *Department of Infectious Diseases, Hamamatsu University School of Medicine, 1-20-1 Handayama, Higashi-ku, Hamamatsu, Shizuoka 431-3192, Japan*

ARTICLE INFO

Article history:
Received 30 March 2012
Returned to author for revisions
23 April 2012
Accepted 25 May 2012

Keywords:
HCV
HCVtcp
Trans-packaging
Single-round infection

ABSTRACT

In this study, we compared the entry processes of *trans*-complemented hepatitis C virus particles (HCVtcp), cell culture-produced HCV (HCVcc) and HCV pseudoparticles (HCVpp). Anti-CD81 antibody reduced the entry of HCVtcp and HCVcc to almost background levels, and that of HCVpp by approximately 50%. Apolipoprotein E-dependent infection was observed with HCVtcp and HCVcc, but not with HCVpp, suggesting that the HCVtcp system is more relevant as a model of HCV infection than HCVpp. We improved the productivity of HCVtcp by introducing adapted mutations and by deleting sequences not required for replication from the subgenomic replicon construct. Furthermore, blind passage of the HCVtcp in packaging cells resulted in a novel mutation in the NS3 region, N1586D, which contributed to assembly of infectious virus. These results demonstrate that our plasmid-based system for efficient production of HCVtcp is beneficial for studying HCV life cycles, particularly in viral assembly and infection.

© 2012 Elsevier Inc. All rights reserved.

Introduction

Over 170 million people worldwide are chronically infected with hepatitis C virus (HCV), and are at risk of developing chronic liver diseases (Hoofnagle, 2002). HCV is an enveloped virus of the family *Flaviviridae*, and its genome is a positive-strand RNA consisting of the 5′-untranslated region (UTR), an open reading frame encoding viral proteins (core, E1, E2, p7, NS2, NS3, NS4A, NS4B, NS5A, and NS5B) and the 3′-UTR (Suzuki et al., 2007).

Host–virus interactions are required during the initial steps of viral infection. It was previously reported that CD81 (Bartosch et al., 2003a, b; McKeating et al., 2004; Pileri et al., 1998), scavenger receptor class B type I (Bartosch et al., 2003a, b; Scarselli et al., 2002), claudin-1 (Evans et al., 2007; Liu et al., 2009) and occludin (Benedicto et al., 2009; Evans et al., 2007; Liu et al., 2009; Ploss et al., 2009) are critical molecules for HCV entry into cells. CD81 interacts with HCV E2 via a second extracellular loop (Bartosch et al., 2003a, b; Hsu et al., 2003) and its role in the internalization process was confirmed (Cormier et al., 2004; Flint et al., 2006). It has also been shown that infectious HCV particles produced in cell cultures (HCVcc) exist as apolipoprotein E (ApoE)-enriched lipoprotein particles (Chang et al., 2007) and that ApoE is important for HCV infectivity (Owen et al., 2009).

Investigation of HCV had been hampered by difficulties in amplifying the virus in vitro before development of robust cell culture systems based on JFH-1 isolates (Lindenbach et al., 2005; Wakita et al., 2005; Zhong et al., 2005). Retrovirus-based HCV pseudoparticles (HCVpp), in which cell entry is dependent on HCV glycoproteins, have been used to study virus entry (Bartosch et al., 2003a; Hsu et al., 2003). Vesicular stomatitis virus (VSV)-based pseudotypic viruses bearing HCV E1 and E2 and replication-competent recombinant VSV encoding HCV envelopes have also been available as surrogate models for studies of HCV infection (Mazumdar et al., 2011; Tani et al., 2007).

It was recently shown that HCV subgenomic replicons can be packaged when structural proteins are supplied in *trans* (Adair et al., 2009; Ishii et al., 2008; Masaki et al., 2010; Steinmann et al., 2008). These *trans*-complemented HCV particles (HCVtcp) are infectious, but support only single-round infection and are unable to spread. Establishment of flexible systems to efficiently produce HCVtcp should contribute to studying HCV assembly, in particular encapsidation of the viral genome, and entry to cells with less stringent biosafety and biosecurity measures. Although single-round infection can be achieved by using the HCVcc system with receptor knock-out

* Corresponding author. Fax: +81 3 5285 1161.
** Corresponding author. Fax: +81 53 435 2338.
E-mail addresses: ryosuke@nih.go.jp (R. Suzuki), tesuzuki@hama-med.ac.jp (T. Suzuki).

0042-6822/$ - see front matter © 2012 Elsevier Inc. All rights reserved.
http://dx.doi.org/10.1016/j.virol.2012.05.033

Please cite this article as: Suzuki, R., et al., *Trans*-complemented hepatitis C virus particles as a versatile tool for study of virus assembly and infection. Virology (2012), http://dx.doi.org/10.1016/j.virol.2012.05.033

cells, the single-round HCVcc system is not suitable for studying virus entry. We previously described plasmid-based production of HCVcc and HCVtcp (Masaki et al., 2010). Here, we demonstrated that HCVtcp production can be enhanced by introducing the previously reported cell-culture adaptive mutations and by deleting sequences not essential for replication in the subgenomic replicon construct. By providing genotype 1b-derived core-to-p7 in addition to intragenotypic viral proteins, chimeric HCVtcp were generated. Furthermore, blind passage of HCVtcp in the packaging cells resulted in the identification of a novel cell culture-adaptive mutation in NS3 that enables us to establish the efficient production of HCVtcp with structural proteins from various strains. Taken together, our system for producing single-cycle infectious HCV particles should be useful in the study of entry and assembly steps of the HCV life cycles. This technology may also have potential to be the basis for the safer vaccine development.

Results

Enhancement of HCVtcp production by adaptive mutations in E2, p7 and NS2 and by deleting sequences not essential for replication from replicon construct

In our HCVtcp system, the RNA polymerase I (Pol I)-driven replicon plasmid, which carries a dicistronic subgenomic luciferase reporter replicon of JFH-1 strain with a Pol I promoter and terminator (pHH/SGR-Luc), as well as a plasmid containing core-NS2 cDNA under the CAG promoter (pCAGC-NS2) were used (Masaki et al., 2010). In an effort to improve the yield of HCVtcp production, cell culture-adaptive mutations in E2 (N417S), p7 (N765D) and NS2 (Q1012R) which were previously selected from serial passage of HCVcc (Russell et al., 2008) were introduced into the core-NS2 expression plasmid (Fig. 1A) (residues are numbered

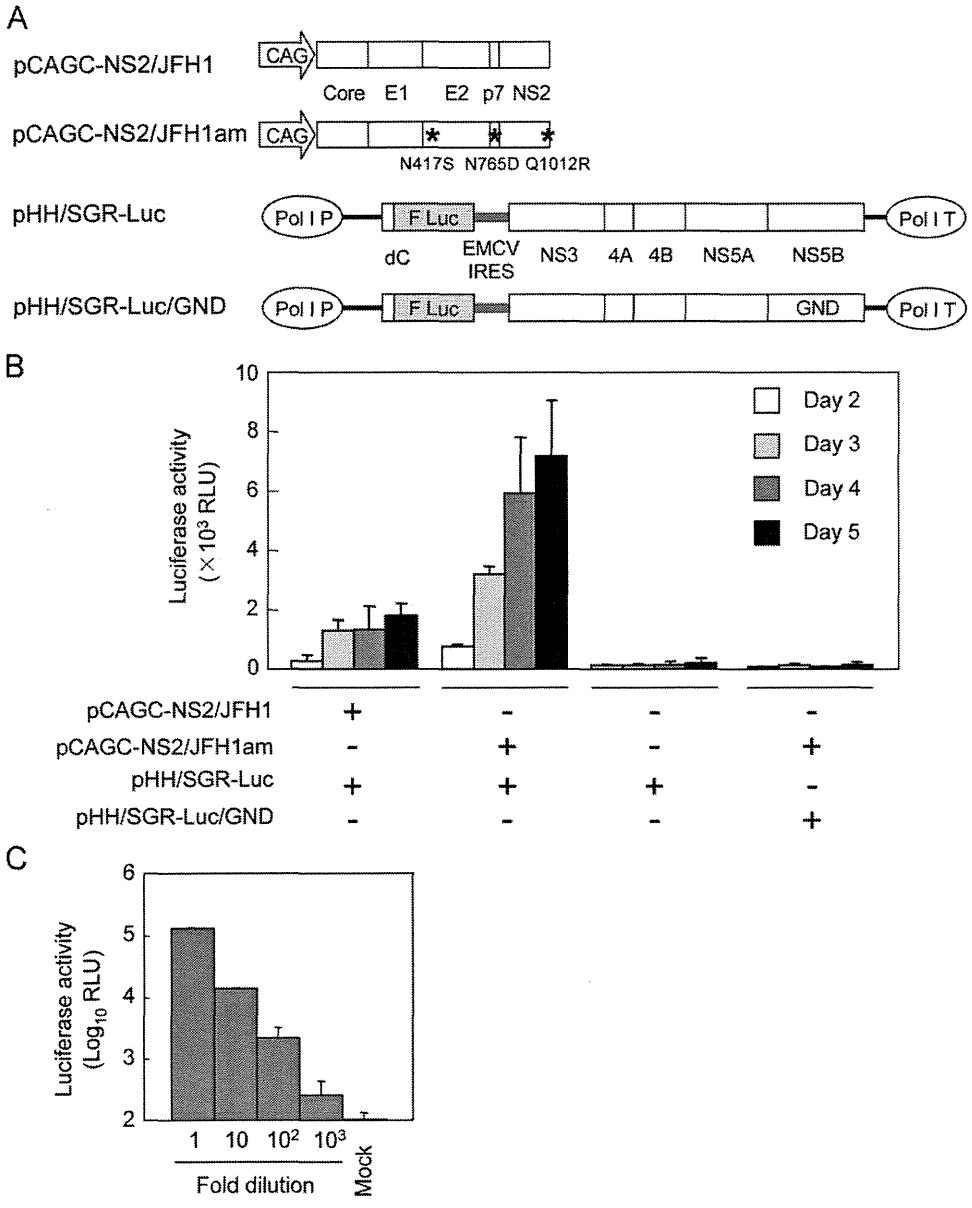

Fig. 1. HCVtcp production by two-plasmid transfection. (A) Schematic representation of plasmids is shown. HCV polyproteins derived from JFH-1 are indicated by white boxes. HCV UTRs are indicated by bold lines. The internal ribosomal entry site from encephalomyocarditis virus (EMCV IRES) is denoted as gray lines. Adaptive mutations are indicated as asterisks. F Luc: firefly luciferase gene; CAG: CAG promoter; Pol I P: RNA polymerase I promoter; Pol I T: RNA polymerase I terminator; GND: replication-deficient GND mutation. (B) Luciferase activity in Huh7.5.1 cells inoculated with supernatant from cells transfected with indicated plasmids at the indicated time points. Data are averages of triplicate values with error bars showing standard deviations. (C) Luciferase activity in cells inoculated with serially diluted HCVtcp.

Please cite this article as: Suzuki, R., et al., *Trans*-complemented hepatitis C virus particles as a versatile tool for study of virus assembly and infection. Virology (2012), http://dx.doi.org/10.1016/j.virol.2012.05.033

according to positions within the JFH-1 polyprotein). Supernatants of cells transfected with plasmids (Fig. 1A) were collected and were used to infect Huh7.5.1 cells, which were analyzed by luciferase assay. Introduction of adaptive mutations (pCAGC-NS2/JFH1am) resulted in more than 4-fold higher production of HCVtcp at 5 day post-transfection, as compared to wild-type (WT) (pCAGC-NS2/JFH1) (Fig. 1B), indicating that the adaptive mutations contribute to enhancing HCVtcp production. To confirm that luciferase activity levels in HCVtcp-infected cells are correlated with the number of infectious particles, Huh7.5.1 cells were inoculated with serial dilutions of HCVtcp. Luciferase activity was well correlated with viral load (Fig. 1C), indicating that luciferase assay in HCVtcp-infected cells can be used to quantify HCV infection.

In order to further explore the efficient production of HCVtcp, we generated replicon constructs that lack the luciferase gene or include the partial coding sequences for structural proteins instead of reporter (Fig. 2A). Replication of each replicon in plasmid-transfected cells was then assessed by Western blotting (Fig. 2B). Among the constructs tested, NS5B levels were lowest in cells expressing pHH/SGR-Luc. NS5B levels in cells replicating other replicons appeared to be comparable. Cells were infected with supernatants of cells transfected with each replicon plasmid, along with pCAGC-NS2/JFH1am, followed by infectious unit assay (Fig. 2C). The highest production of HCVtcp was obtained from cells transfected with pHH/SGR, where the luciferase sequence was deleted from pHH/SGR-Luc, thus suggesting that deletion of the sequence not essential for RNA replication in the replicon may contribute to enhancing HCVtcp production.

Production of chimeric HCVtcp by providing heterologous core-p7

In order to elucidate whether *trans*-encapsidation of JFH-1 replicon can be achieved by providing core-p7 from other HCV strains, core-NS2 plasmids were constructed (Fig. 3A). In these plasmids, core through the N-terminal 33 aa of NS2, which contains transmembrane domain 1 of NS2, was derived from either H77c (genotype 1a), THpa (genotype 1b), Con1 (genotype 1b) or J6 (genotype 2a) strain. Residual NS2 was derived from JFH-1, as described previously (Pietschmann et al., 2006). HCVtcp was efficiently produced by core-p7 of J6 and THpa strains, but its production was less efficient in the case of Con1 strain. *Trans*-packaging was not detectable when core-p7 of H77c strain was used (Fig. 3C). Among HCV strains tested, difference in luciferase activity levels in HCVtcp-infected cells (Fig. 3C) were in agreement with that in the viral RNA levels in the culture supernatants of the transfected cells (Fig. 3B). Although the efficacy of *trans*-complementation was variable among strains, chimeric HCVtcp can be generated by providing genotype 1b-derived core-p7 in addition to intragenotypic viral proteins, and was used in subsequent studies.

ApoE- and CD81-dependent infection by HCVtcp

There is accumulating evidence that apolipoproteins, particularly ApoE, contribute to HCV production and infectivity (Chang et al., 2007; Owen et al., 2009). To determine whether ApoE is involved in infection of target cells by HCVtcp, we infected cells in the presence of increasing concentrations of anti-ApoE antibody.

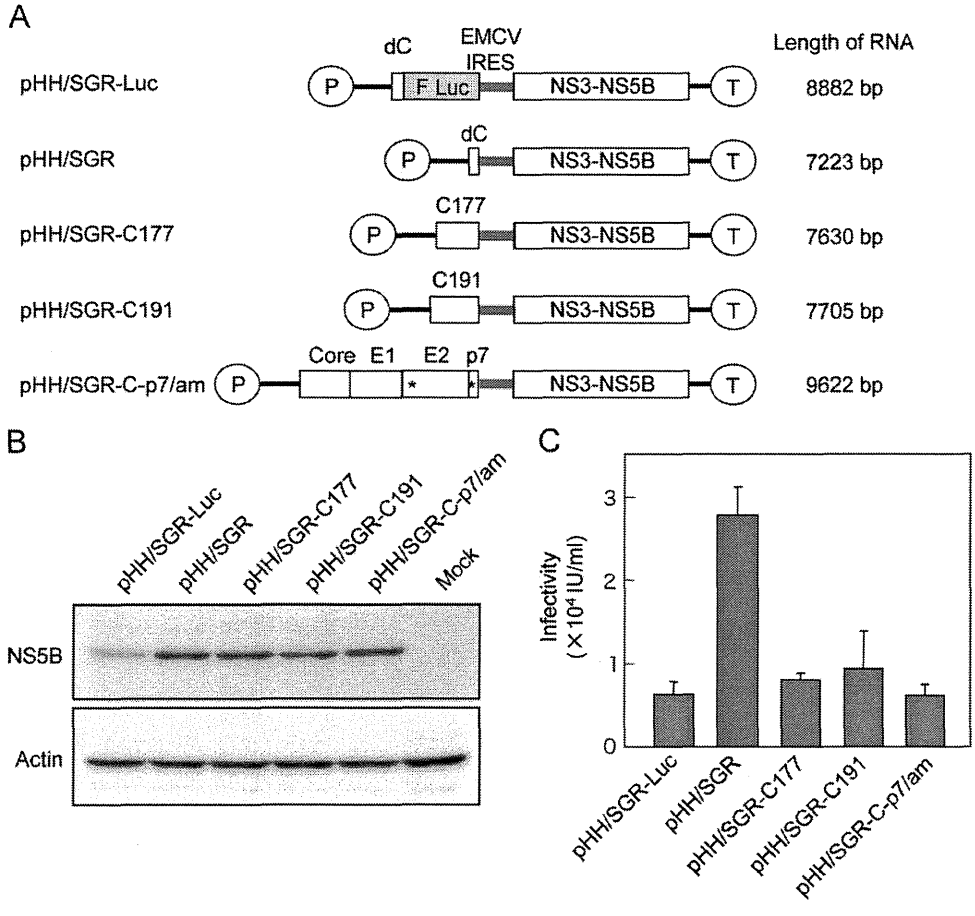

Fig. 2. Production of HCVtcp with different replicon constructs. (A) Schematic representation of plasmids used for production of HCVtcp. Deduced length of transcribed RNA from each construct is shown on the right. HCV polyproteins from JFH-1 strain are indicated by open boxes. HCV UTRs are indicated by bold lines. The EMCV IRES is denoted by gray bars. Adaptive mutations are indicated by asterisks. F Luc: firefly luciferase gene; P: RNA polymerase I promoter; T: RNA polymerase I terminator. (B) Detection of NS5B and actin in Huh7.5.1 cells transfected with indicated plasmids at 4 day post-transfection. (C) Infectivity of culture supernatants from cells transfected with indicated replicon plasmids along with pCAGC-NS2/JFH1am at 4 day post-transfection.

Please cite this article as: Suzuki, R., et al., *Trans*-complemented hepatitis C virus particles as a versatile tool for study of virus assembly and infection. Virology (2012), http://dx.doi.org/10.1016/j.virol.2012.05.033

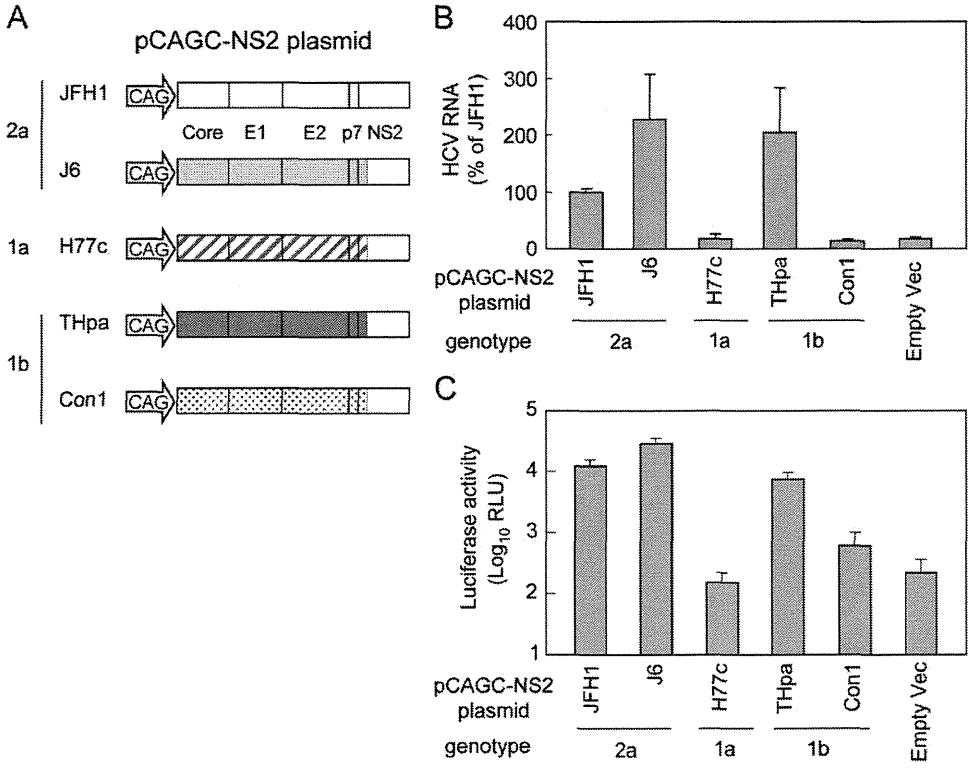

Fig. 3. HCVtcp production with structural proteins from various strains. (A) Schematic representation of plasmids used. HCV polyproteins of JFH-1, J6, H77c, THpa and Con1 strain are shown in the open box, bright gray box, box with diagonal lines, dark gray box and dotted box, respectively. (B) Relative levels of HCV RNA in the supernatant from cells transfected with indicated plasmids along with pHH/SGR-Luc. (C) Luciferase activity in cells inoculated with supernatant from cells transfected with indicated plasmids along with pHH/SGR-Luc at 4 day post-transfection.

pCAGC-NS2/THpa and pCAGC-NS2/JFH1am were used as core-NS2 plasmids for HCVtcp production carrying core-p7 derived from genotypes 1b and 2a (HCVtcp-1b and HCVtcp-2a, respectively). HCVpp derived from JFH-1 and VSVpp were generated and used for comparison. Infection with HCVtcp-1b or HCVtcp-2a was blocked by anti-ApoE antibody in a dose-dependent manner. In contrast, anti-ApoE antibody did not affect infection with HCVpp and VSVpp (Fig. 4A).

The CD81 dependence of infection was also compared between HCVtcp and HCVpp (Fig. 4B). Anti-CD81 antibody inhibited the entry of HCVtcp-1b, HCVtcp-2a, and HCVpp in a dose-dependent manner. The antibody had no effect on VSVpp infection. HCVtcp infection appears to be more sensitive to anti-CD81 antibody when compared with HCVpp infection; more than 60% inhibition was observed at 0.08 μg/mL anti-CD81 antibody for HCVtcp-1b and HCVtcp-2a, whereas approximately 50% inhibition was observed for HCVpp at 2 μg/mL antibody. Neutralization of HCVcc by anti-ApoE and anti-CD81 antibodies was also determined. Antibodies blocked HCVcc infection (Fig. 4C and D), as observed with HCVtcp. These results suggest that ApoE, as well as CD81, play an important role in HCVtcp infection. Thus, HCVtcp may be more useful for evaluating the HCV entry process than HCVpp.

Identification of novel culture-adaptive mutation in NS3 by serial passage of HCVtcp in packaging cells

The HCVtcp system was further applied to analyses of genetic changes during serial passages in target cells. As an initial attempt, supernatants of cells co-transfected with pCAGC-NS2/JFH1am and pHH/SGR were inoculated into Huh7.5.1 cells transiently transfected with pCAGC-NS2/JFH1am. However, infectious titer was lost after repeated inoculation, likely due to low HCVtcp titers and low efficiency of plasmid transduction (data not shown). To overcome this, we utilized recombinant adenovirus vectors (rAdVs) to provide core-NS2. As we were not able to obtain rAdV directly expressing core-NS2, conditional transgene expression based on a Cre-loxP strategy was employed (Kanegae et al., 1995). We constructed an rAdV containing core-NS2 gene downstream of a stuffer DNA flanked by a pair of loxP sites (AxCALNLH-CNS2). When cells were doubly infected with AxCALNLH-CNS2 and the Cre-expressing rAdV, AxCANCre (Kanegae et al., 1995), the Cre-mediated excisional deletion removed the stuffer DNA, resulting in core-NS2 expression under control of the CAG promoter (Fig. 5A). As expected, tightly regulated production of HCVtcp was observed. The cells infected with AxCANCre and AxCALNLH-CNS2 along with transduction of pHH/SGR-Luc produced HCVtcp at high levels. Production of HCVtcp was undetectable when either AxCANCre or AxCALNLH-CNS2 was not infected (Fig. 5B). The Cre-mediated rAdV expression system appears to have yielded considerably higher production of HCVtcp when compared with the settings for plasmid co-transfection.

Supernatants from cells in which core-NS2 was expressed using rAdVs and the subgenomic RNA derived from pHH/SGR replicated were inoculated into cells infected with AxCALNLH-CNS2 and AxCANCre (Fig. 6A). Blind passage was performed by sequentially transferring culture supernatants to cells infected with the above rAdVs. The two independent 10 blind passages (p10) showed virus titers of $>1\times10^6$ IU/mL, which were markedly higher than those of the passage 0 (p0) stock cultures (4×10^4 IU/mL). Side-by-side infection analysis revealed that the HCVtcp p10 #1 achieved a virus titer approximately 36 times higher than that of HCVtcp p0 on the packaging cells at 6 day post-infection (Fig. 6B). Sequencing of the entire replicon in the supernatants at p10 in two independent experiments revealed

Please cite this article as: Suzuki, R., et al., *Trans*-complemented hepatitis C virus particles as a versatile tool for study of virus assembly and infection. Virology (2012), http://dx.doi.org/10.1016/j.virol.2012.05.033

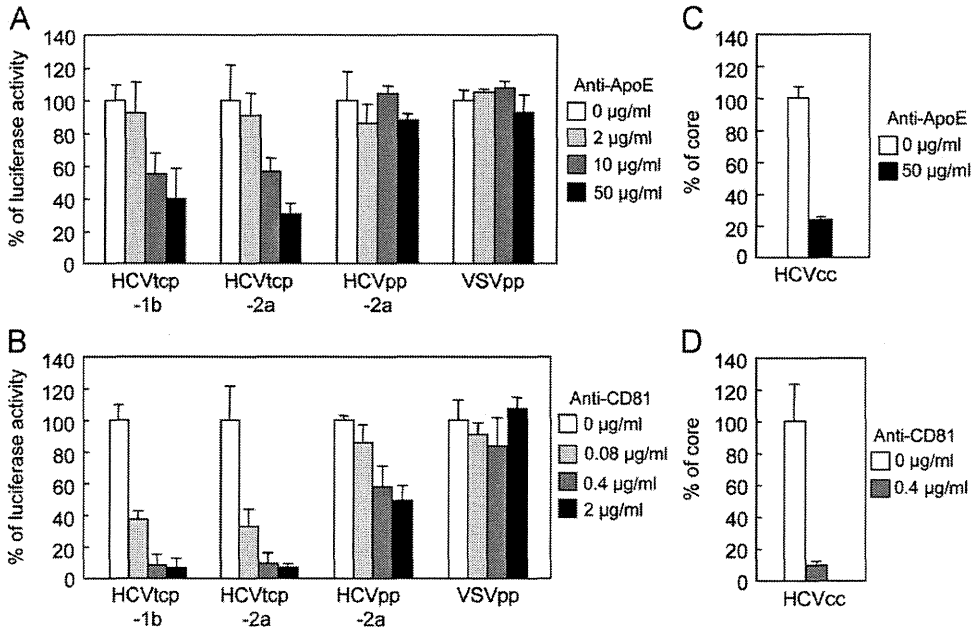

Fig. 4. Effects of anti-ApoE and anti-CD81 antibodies on HCV entry. (A) Aliquots of virus sample were incubated with increasing concentrations of anti-ApoE antibodies for 1 h and were then added to Huh7.5.1 cells. Luciferase activity was determined at 72 h post-infection and is expressed relative to activity without antibodies (white bar). (B) Huh7.5.1 cells were preincubated for 1 h with increasing concentrations of anti-CD81 antibodies, followed by inoculating virus samples. Luciferase activity was determined and expressed as shown in (A). (C) Aliquots of HCVcc were incubated with anti-ApoE antibodies for 1 h and were then added to Huh7.5.1 cells at an MOI of 0.05. Intracellular core levels were quantitated at 24 h post-infection and are expressed relative to levels without antibodies (white bar). (D) Huh7.5.1 cells were preincubated for 1 h with anti-CD81 antibodies. HCVcc infection and measurement of core proteins were performed as indicated in (C).

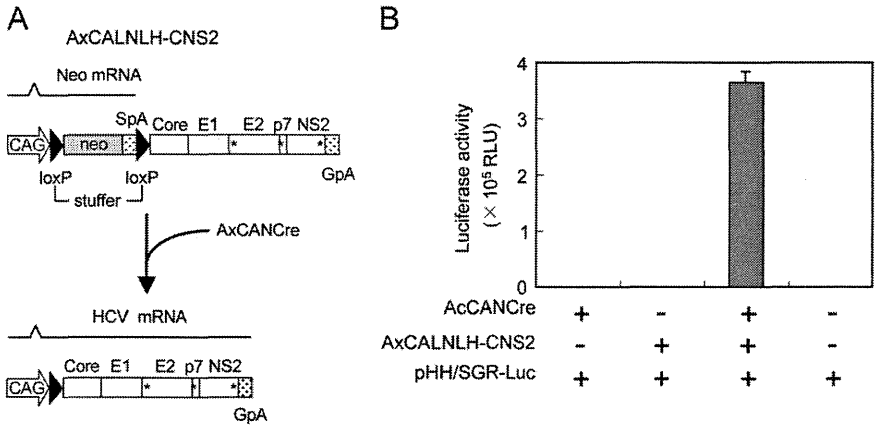

Fig. 5. Transgene activation mediated by rAdVs expressing Cre recombinase under control of CAG promoter. (A) Cre recobminase expressed by AxCANCre recognizes a pair of its target sequences loxP in AxCALNLH-CNS2, and removes the stuffer region resulting in expression of HCV core-NS2 polyprotein by CAG promoter. CAG: CAG promoter; SpA: SV40 early polyA signal; GpA: rabbit b-globin poly(A) signal. (B) Luciferase activity in Huh7.5.1 cells inoculated with 4-day post-transfection culture supernatant from cells transfected with pHH/SGR-Luc, and then infected with indicated rAdVs.

that both passaged HCVtcp had an identical nonsynonymous mutation in the NS3 region (N1586D) (Fig. 6C).

In order to examine the role of NS3 mutation identified on HCV RNA replication and on HCVtcp production, the N1586D mutation was introduced into pHH/SGR-Luc. Luciferase activities of the N1586D-mutated replicon were apparently lower than those of the WT-replicon, thus suggesting that the NS3 mutation reduced viral RNA replication (Fig. 7A). HCV RNA levels in the supernatants of cells transfected with WT- or mutant replicon plasmid along with pCAGC-NS2/JFH1am and luciferase activity in cells inoculated with supernatants from the transfected cells were then determined (Fig. 7B). The viral RNA level secreted from cells replicating the N1586D-mutated replicon was lower than that from cells replicating WT replicon (Fig. 7B, left). By contrast, a significantly higher infectivity of HCVtcp produced from the mutant replicon-cells was observed, as compared to WT replicon-cells (Fig. 7B, right), suggesting that the adaptive mutation increased the specific infectivity (almost 9-fold) of the virus particles. To further determine whether the N1586D mutation affects infectious viral assembly and/or virus release, we used the CD81-negative Huh-7 subclone, Huh7-25 (Akazawa et al., 2007), which may produce infectious particles, but is not susceptible to HCV entry due to a lack of CD81 expression, therefore allowing us to examine viral assembly and release without the influence of reinfection by produced HCVtcp. Measurement of intracellular and extracellular HCVtcp indicated that Huh7-25 cells replicating the N1586D-mutated replicon produced more infectious virus than WT in both supernatants and cell lysates (Fig. 7C). Thus, it can be concluded that the N1586D mutation contributes to enhanced infectious viral assembly, not RNA replication. We could not exclude the possibility that N1586D mutation affects virus release, since the mutation enhanced extracellular virus titers more than did the intracellular titer.

Please cite this article as: Suzuki, R., et al., *Trans*-complemented hepatitis C virus particles as a versatile tool for study of virus assembly and infection. Virology (2012), http://dx.doi.org/10.1016/j.virol.2012.05.033

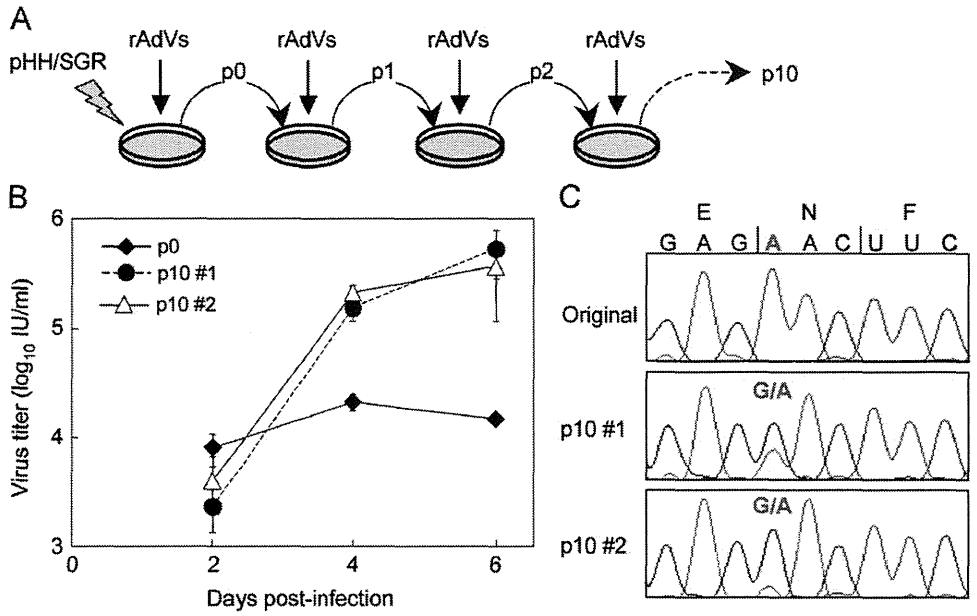

Fig. 6. Genotypic changes in HCVtcp following blind passage. (A) Experimental procedure for blind passage of HCVtcp. Huh7.5.1 cells were transfected with pHH/SGR and were doubly infected with AxCANCre and AxCALNLH-CNS2. Culture fluids were collected and were inoculated into cells infected with AxCANCre and AxCALNLH-CNS2. These procedures were repeated 10 times with two independent samples (#1 and #2). (B) Growth curves of HCVtcp p0 and p10 on Huh7.5.1 cells expressing core-NS2. Cells were infected with HCVtcp at an MOI of 0.05, and medium was collected at the indicated time points and subjected to titration. (C) Nucleotide sequences of original and blind-passaged replicons from HCVtcp. Nucleotides of mutated position are shown in red and bold.

The impact of the N1586D mutation on production of intra- and intergenotypic HCVtcp chimeras was also investigated. The N1586D mutation in the replicon enhanced the production of chimeric HCVtcp by providing core-p7 from all strains examined, although not statistically significant in THpa, and Con1 strains (Fig. 7D). Finally, to determine whether the N1586D mutation was responsible for enhancing HCVcc production, this mutation was introduced into pHHJFH1, which carries the full-length wild-type JFH-1 cDNA (Masaki et al., 2010), yielding pHHJFH1N1586D. The virus titer obtained from cells transfected with the pHHJFH1N1586D was significantly higher than that of WT (Fig. 7E), thus demonstrating that the N1586D mutation enhances yields of HCVcc, in addition to HCVtcp.

Discussion

Single-round infectious viral particles generated by *trans*-packaging systems are considered to be valuable tools for studying virus life cycles, particularly the steps related to entry into target cells, assembly and release of infectious particles. However, limited HCV strains have been applied for the efficient production of HCVtcp to date. In this study, we improved the HCVtcp system in order to enhance the productivity of infectious particles. Production of chimeric HCVtcp by providing genotype 1b-derived core-p7, in addition to intragenotypic viral proteins, was also confirmed. Furthermore, we exploited the system to investigate genetic changes during serial passage of target cells and identified a novel cell culture-adaptive mutation in NS3, which also contributes to enhance the productivity of HCVtcp.

HCVpp (Bartosch et al., 2003a; Hsu et al., 2003) has proven to be a valuable surrogate system by which the study of viral and cellular determinants of the viral entry pathway is possible. Early steps of HCV infection, including the role of HCV glycoprotein heterodimers, receptor binding, internalization and pH-dependent endosomal fusion, have been at least in part mimicked by HCVpp (Lavie et al., 2007). However, as HCVpp is generated in non-hepatic cells such as the human embryo kidney cells 293T, it is likely that the cell-derived component(s) of HCVpp differ from those of HCVcc. Hepatocytes play a role in maintaining lipid homeostasis in the body by assembling and secreting lipoproteins, including VLDL. It is highly likely that HCV exploits lipid synthesis pathways, as there is a tight link between virion formation and VLDL synthesis. Down-regulation of ApoE considerably reduces HCV production (Benga et al., 2010; Chang et al., 2007; Hishiki et al., 2010; Jiang and Luo, 2009; Owen et al., 2009). Infectivity of HCVcc is also neutralized by anti-ApoE antibodies (Chang et al., 2007). These data suggest that ApoE is important for HCV infectivity. Furthermore, Niemann-Pick C1-like 1 (NPC1L1), involving cholesterol uptake receptor, was recently identified as a host factor for HCV entry (Sainz et al., 2012). Knockdown of NPC1L1 had no effect on the entry of HCVpp whereas HCVcc entry was impaired, possibly due to different cholesterol content of these particles. Here, we found that the anti-ApoE antibody neutralized infection by HCVtcp and HCVcc, but not by HCVpp (Fig. 4A and C), thus suggesting that biogenesis and/or secretion pathways of VLDL are involved in HCVtcp similarly to HCVcc, but not in HCVpp.

We also observed that infectivity of HCVtcp and HCVcc is more efficiently neutralized by the anti-CD81 antibody, as compared to that of HCVpp (Fig. 4B and D). It has recently been reported that E2 of HCVcc contained both high-mannose-type and complex-type glycans, whereas most of the glycans on HCVpp-associated E2 were complex-type, which is matured by Golgi enzymes (Vieyres et al., 2010). Mutational analysis of the N-linked glycosylation sites in E1/E2 demonstrated that several glycans on E2 may affect the sensitivity of HCVpp against antibody neutralization, as well as access of CD81 to its binding site on E2 (Helle et al., 2010). The differences in sensitivity between HCVtcp and HCVpp to neutralization by anti-CD81 antibody observed here may be due to differences in carbohydrate composition of HCV glycoproteins during expression and processing of E1/E2 in cells and morphogenesis of HCVtcp and HCVpp.

By analyzing the various replicons for *trans*-packaging, we observed the highest production of HCVtcp with replicons from pHH/SGR, which lacked sequences not essential for RNA

Please cite this article as: Suzuki, R., et al., *Trans*-complemented hepatitis C virus particles as a versatile tool for study of virus assembly and infection. Virology (2012), http://dx.doi.org/10.1016/j.virol.2012.05.033

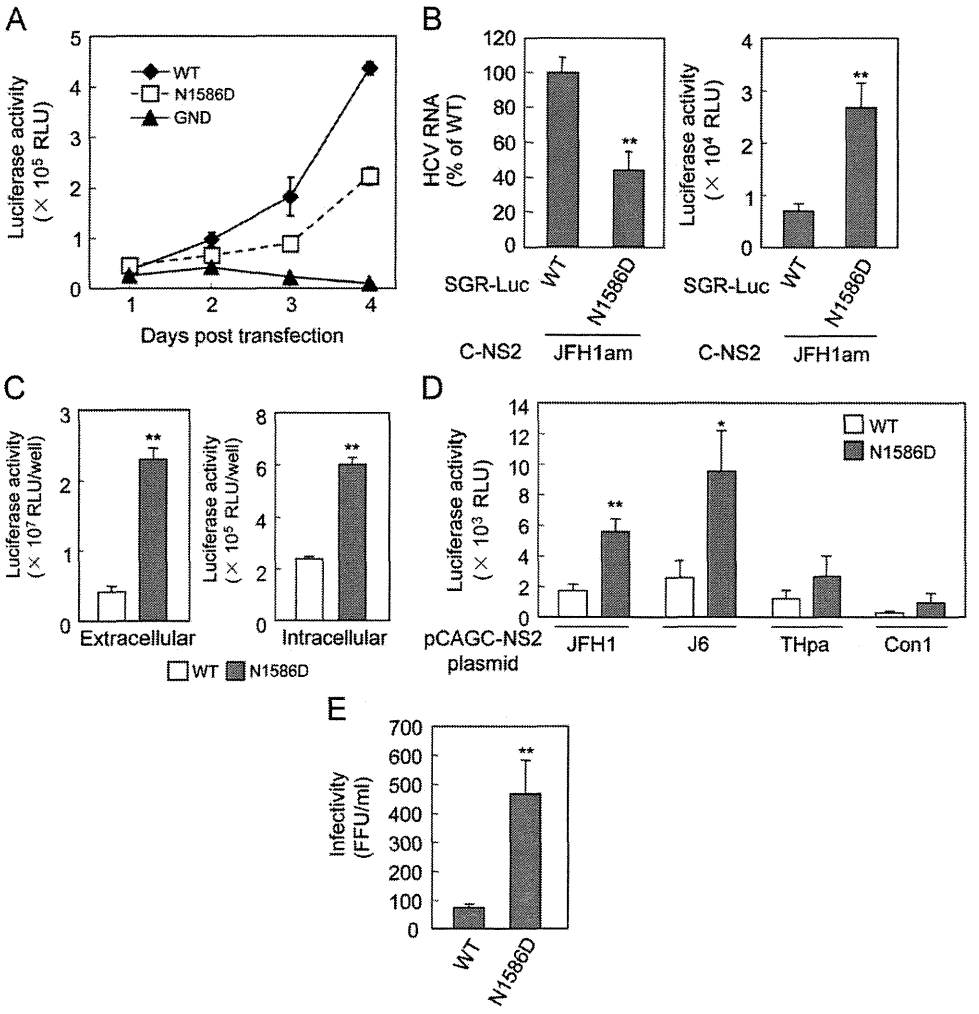

Fig. 7. Effects of N1586D mutation on RNA replication and production of HCVtcp or HCVcc. (A) RNA replication of replicons in cells transfected with pHH/SGR-Luc (WT) or N1586D mutant. Luciferase activities at 1 to 4 day post-transfection were determined. (B) Relative levels of HCV RNA in the supernatants from cells transfected with pHH/SGR-Luc (WT) or N1586D mutant plasmid along with pCAGC-NS2/JFH1am were shown in the left panel. Luciferase activities in cells inoculated with supernatants from cells transfected with indicated plasmids at 4 day post-transfection were shown in the right panel. (C) Luciferase activity in cells inoculated with supernatant and cell lysates from Huh7-25 cells transfected with pHH/SGR-Luc (WT) or N1586D mutant plasmid along with pCAGC-NS2/JFH1am at 5 day post-transfection. (D) Luciferase activity in cells inoculated with culture supernatant from cells transfected with pHH/SGR-Luc (WT) or N1586D mutant plasmid along with indicated core-NS2 plasmids at 4 day post-transfection. (E) Infectivity of supernatant from cells transfected with pHH/JFH1 (WT) or its derivative plasmid containing N1586D mutation at 6 day post-transfection. Statistical differences between WT and N1586D were evaluated using Student's *t*-test. $^{*}p < 0.05$, $^{**}p < 0.005$ vs. WT.

replication, while less efficient productivity was observed from pHH/SGR-Luc, pHH/SGR-C177, pHH/SGR-C191 and pHH/SGR-C-p7/am (Fig. 2C). Differences in the replication efficiency of the replicon do not appear to be a major determinant for HCVtcp productivity, at least in the present settings, as all replicon constructs except pHH/SGR-Luc replicated at similar levels, as confirmed by Western blotting (Fig. 2B). Although the shorter viral genome sequence may offer advantages over the longer sequence, further investigation is required in order to understand the molecular mechanisms underlying viral genome packaging. By comparing pHH/SGR vs. pHH/SGR-C177, pHH/SGR-C191 and pHH/SGR-C-p7/am, it is likely that the expression of the structural protein in *cis* does not increase HCVtcp production when sufficient amounts of structural proteins are supplied in *trans*.

Blind passage of HCVtcp in packaging cells infected with rAdVs providing core-NS2 enabled us to identify a novel culture-adaptive mutation in NS3. The N-terminal third of NS3 forms a serine protease, together with NS4A, and its C-terminal two-thirds exhibits RNA helicase and RNA-stimulated NTPase activities. In addition, similarly to flaviviruses (Kummerer and Rice, 2002; Liu et al., 2002), it is now apparent that HCV NS3 is also involved in viral morphogenesis (Han et al., 2009; Ma et al., 2008), although its precise role and underlying molecular mechanism(s) have not fully been elucidated. Two cell-culture adaptive NS3 mutations which are involved in HCV assembly have been identified. The Q1251L mutation in helicase subdomain 1 resulted in approximately 30-fold higher production of HCV without affecting NS3 enzymatic activities (Ma et al., 2008). The M1290K adaptive mutation was also located in subdomain 1 of the NS3 helicase (Han et al., 2009). The N1586D mutation identified here was located in subdomain 3 of helicase. Analogous to Q1251L and M1290K, the N1586D mutation enhanced the infectious viral assembly by increasing specific infectivity without affecting the efficiency of viral RNA replication. Considering the possibility that NS3 plays a role in linking between the viral replicase and assembly sites (Jones et al., 2011), it is likely that NS3 helicase is one of the determinants for interaction with the structural proteins. Our results, together with earlier studies, suggest that chimeric and defective mutations as well as supplying the viral components in *trans*, function as selective pressures in virion assembly.

In summary, we have established a plasmid-based reverse genetics for efficient production of HCVtcp with structural

Please cite this article as: Suzuki, R., et al., *Trans*-complemented hepatitis C virus particles as a versatile tool for study of virus assembly and infection. Virology (2012), http://dx.doi.org/10.1016/j.virol.2012.05.033

proteins from various strains. Single-round infectious HCVtcp can complement the HCVcc and HCVpp systems as a valuable tool for the study of HCV life cycles.

Materials and methods

Cells

Huh7 derivative cell line Huh7.5.1 and Huh7-25 were maintained in Dulbecco modified Eagle medium (DMEM) supplemented with nonessential amino acids, 100 U of penicillin/mL, 100 μg of streptomycin/mL, and 10% fetal bovine serum at 37 °C in a 5% CO_2 incubator.

Plasmids

Plasmids pHHJFH1, pHH/SGR-Luc, pHH/SGR-Luc/GND and pCAG/C-NS2 were as described previously (Masaki et al., 2010). In this study, plasmid pCAG/C-NS2 was designated as pCAGC-NS2/JFH. The plasmid pCAGC-NS2/JFHam having adaptive mutations in E2 (N417S), p7 (N765D), and NS2 (Q1012R) in pCAGC-NS2/JFH was constructed by oligonucleotide-directed mutagenesis. These mutations were also introduced in pHHJFH1, resulting in pHHJFH1am. To generate core-NS2 expression plasmids with different strains of HCV, the cDNA coding core to the first transmembrane region of NS2 (33 amino acids) in pCAGC-NS2/JFH was replaced with the corresponding sequence of the J6 (Lindenbach et al., 2005), H77c (Yanagi et al., 1997), THpa (Shirakura et al., personal communication) and Con1 (Koch and Bartenschlager, 1999) strains. The THpa sequence contained the P to A mutation at 328 aa at E1 in the original TH strain. To generate pHH/SGR, pHH/SGR-Luc was digested with MluI and PmeI, followed by Klenow enzyme treatment and self-ligation to delete the luciferase coding sequence. To generate pHH/SGR-C177, pHH/SGR-C191 and pHH/SGR-C-p7/am, cDNA coding the partial core and luciferase in pHH/SGR-Luc were replaced with coding sequences for mature core (177aa), full-length core (191aa) or core-p7 polyprotein containing adaptive mutations in E2 and p7, respectively. The selected NS3 mutation (N1586D) was introduced into pHH/SGR-Luc and pHHJFH1 by oligonucleotide-directed mutagenesis.

Generation of viruses

HCVcc and HCVtcp were generated as described previously (Masaki et al., 2010). For the production of HCVpp-2a, plasmid pcDNAdeltaC-E1-E2(JFH1)am having adaptive mutations in E2 (N417S) in pcDNAdeltaC-E1-E2(JFH1) (Akazawa et al., 2007) was constructed by oligonucleotide-directed mutagenesis. Murine leukemia virus pseudotypes with VSV G glycoprotein expressing luciferase reporter (VSVpp) were generated in accordance with previously described methods (Akazawa et al., 2007; Bartosch et al., 2003a).

Luciferase assay

Huh7.5.1 cells were seeded onto a 24-well plate at a density of 3×10^4 cells/well 24 h prior to inoculation with reporter viruses. Cells were incubated for 72 h, followed by lysis with 100 μL of lysis buffer. Luciferase activity of the cells was determined using a luciferase assay system (Promega, Madison, WI). All luciferase assays were performed in triplicate.

Quantification of HCV infectivity and HCV RNA

To determine the titers of HCVtcp and HCVcc, Huh7.5.1 cell monolayers prepared in multi-well plates were incubated with dilutions of samples and then replaced with media containing 10% FBS and 0.8% carboxymethyl cellulose. Following incubation for 72 h, monolayers were fixed and immunostained with rabbit polyclonal anti-NS5A antibody, followed by Alexa Fluor 488-conjugated anti-rabbit secondary antibody (Invitrogen), and stained foci or individual cells were counted and used to calculate a titer of focus-forming units (FFU)/mL for spreading infections or infectious units (IU)/mL for non-spreading infections. For intracellular infectivity, the cell pellet was resuspended in culture media, and cells were lysed by four freeze–thaw cycles. Cell debris was pelleted by centrifugation for 5 min at 4000 rpm. Supernatant was collected and used for titration. To determine the amount of HCV RNA in culture supernatants, RNA was extracted from 140 μL of culture medium by QIAamp Viral RNA Mini Kit (QIAGEN, Valencia, CA) and treated with DNase (TURBO DNase; Ambion, Austin, TX) at 37 °C for 1 h. Extracted RNA was further purified by using an RNeasy Mini Kit, which includes RNase-free DNase digestion (QIAGEN). Copy numbers of HCV RNA were determined by real-time quantitative reverse transcription-PCR as described previously (Wakita et al., 2005).

Antibodies

Mouse monoclonal antibodies against actin (AC-15) and CD81 (JS-81) were obtained from Sigma (St. Louis, MO) and BD Biosciences (Franklin Lakes, NJ), respectively. Goat polyclonal antibody to ApoE (LV1479433) was obtained from Millipore (Tokyo, Japan). Anti-NS5A and anti-NS5B antibodies were rabbit polyclonal antibody against synthetic peptides.

Neutralization assay

For neutralization experiments with anti-CD81 antibody, Huh7.5.1 cells were incubated with dilutions of anti-CD81 antibody for 1 h at 37 °C. Cells were then infected with viruses for 5 h at 37 °C. For neutralization experiments with anti-ApoE antibody, viruses were incubated with various concentrations of anti-ApoE antibody at room temperature for 1 h and cells were infected with viruses for 5 h at 37 °C. Following infection, supernatant was removed and cells were incubated with culture medium, and luciferase activity was determined at 3 day post-infection for HCVtcp and pseudotyped viruses. For neutralization experiments with HCVcc generated with pHHJFH1am, a multiplicity of infection (MOI) of 0.05 was used for inoculation, and intracellular core protein levels were monitored by ELISA (Ortho Clinical Diagnostics) at 24 h post-infection.

Immunoblotting

Transfected cells were washed with PBS and incubated with lysis buffer (50 mM Tris–HCl, pH 7.4, 300 mM NaCl, 1% triton X-100). Lysates were then sonicated for 5 min and were added to the same volume of SDS sample buffer. Protein samples were boiled for 10 min, separated by SDS-PAGE, and transferred to PVDF membrane. After blocking, membranes were probed with first antibodies, followed by incubation with peroxidase-conjugated secondary antibody. Antigen–antibody complexes were visualized using an enhanced chemiluminescence detection system (Super Signal West Pico Chemiluminescent Substrate; PIERCE, Rockford, IL), in accordance with the manufacturer's protocols.

Please cite this article as: Suzuki, R., et al., *Trans*-complemented hepatitis C virus particles as a versatile tool for study of virus assembly and infection. Virology (2012), http://dx.doi.org/10.1016/j.virol.2012.05.033

Generation of recombinant adenoviruses

rAdV, AxCANCre, expressing Cre recombinase tagged with nuclear localization signal under CAG promoter was prepared as described previously (Baba et al., 2005). The target rAdV AxCALNLH-CNS2 expressing HCV core-NS2 polyprotein with adaptive mutations in E2, p7 and NS2 was generated as follows. Cosmid pAxCALNLwit2 is identical to pAxCALNLw (Sato et al., 1998), except that both the terminal sequences of the rAdV genome are derived from pAxCAwit2 (Fukuda et al., 2006). The core-NS2 fragment obtained from pCAGC-NS2/JFH1am by StuI-EcoRI digestion and subsequent Klenow treatment was inserted into the SwaI site of pAxCALNLwit2. The resultant cosmid pAxCALNLH-CN2it2 was digested with PacI and transfected into 293 cells to generate rAdV AxCALNLH-CNS2.

Preparation of packaging cells for HCVtcp

Huh7.5.1 cells were coinfected with AxCANCre at an MOI of 1 and AxCALNLH-CNS2 at an MOI of 3 for expression of JFH-1 core-NS2 polyprotein containing the adaptive mutations in E2, p7 and NS2.

RNA preparation, RT-PCR and sequencing

Total cellular RNA was extracted with TRIzol reagent (Invitrogen, Carlsbad, CA), and subjected to reverse transcription with random hexamer and Superscript III reverse transcriptase (Invitrogen). Three fragments of HCV cDNAs that cover the entire HCV subgenomic replicon genome, were amplified by nested PCR with TaKaRa Ex Taq polymerase (Takara, Shiga, Japan). Amplified products were separated by agarose gel electrophoresis, and were used for direct DNA sequencing.

Acknowledgments

We are grateful to Francis V. Chisari (The Scripps Research Institute) for providing Huh7.5.1 cells. We thank M. Sasaki, M. Matsuda, and T. Date for their technical assistance, and T. Mizoguchi for the secretarial work. We also thank T. Masaki for their helpful discussions. This work was supported in part by grants-in-aid from the Ministry of Health, Labor, and Welfare and the Ministry of Education, Culture, Sports, Science, and Technology, Japan.

References

Adair, R., Patel, A.H., Corless, L., Griffin, S., Rowlands, D.J., McCormick, C.J., 2009. Expression of hepatitis C virus (HCV) structural proteins in trans facilitates encapsidation and transmission of HCV subgenomic RNA. J. Gen. Virol. 90 (Part 4), 833–842.

Akazawa, D., Date, T., Morikawa, K., Murayama, A., Miyamoto, M., Kaga, M., Barth, H., Baumert, T.F., Dubuisson, J., Wakita, T., 2007. CD81 expression is important for the permissiveness of Huh7 cell clones for heterogeneous hepatitis C virus infection. J. Virol. 81 (10), 5036–5045.

Baba, Y., Nakano, M., Yamada, Y., Saito, I., Kanegae, Y., 2005. Practical range of effective dose for Cre recombinase-expressing recombinant adenovirus without cell toxicity in mammalian cells. Microbiol. Immunol. 49 (6), 559–570.

Bartosch, B., Dubuisson, J., Cosset, F.L., 2003a. Infectious hepatitis C virus pseudoparticles containing functional E1-E2 envelope protein complexes. J. Exp. Med. 197 (5), 633–642.

Bartosch, B., Vitelli, A., Granier, C., Goujon, C., Dubuisson, J., Pascale, S., Scarselli, E., Cortese, R., Nicosia, A., Cosset, F.L., 2003b. Cell entry of hepatitis C virus requires a set of co-receptors that include the CD81 tetraspanin and the SR-B1 scavenger receptor. J. Biol. Chem. 278 (43), 41624–41630.

Benedicto, I., Molina-Jimenez, F., Bartosch, B., Cosset, F.L., Lavillette, D., Prieto, J., Moreno-Otero, R., Valenzuela-Fernandez, A., Aldabe, R., Lopez-Cabrera, M., Majano, P.L., 2009. The tight junction-associated protein occludin is required for a postbinding step in hepatitis C virus entry and infection. J. Virol. 83 (16), 8012–8020.

Benga, W.J., Krieger, S.E., Dimitrova, M., Zeisel, M.B., Parnot, M., Lupberger, J., Hildt, E., Luo, G., McLauchlan, J., Baumert, T.F., Schuster, C., 2010. Apolipoprotein E interacts with hepatitis C virus nonstructural protein 5A and determines assembly of infectious particles. Hepatology 51 (1), 43–53.

Chang, K.S., Jiang, J., Cai, Z., Luo, G., 2007. Human apolipoprotein E is required for infectivity and production of hepatitis C virus in cell culture. J. Virol. 81 (24), 13783–13793.

Cormier, E.G., Tsamis, F., Kajumo, F., Durso, R.J., Gardner, J.P., Dragic, T., 2004. CD81 is an entry coreceptor for hepatitis C virus. Proc. Natl. Acad. Sci. USA 101 (19), 7270–7274.

Evans, M.J., von Hahn, T., Tscherne, D.M., Syder, A.J., Panis, M., Wolk, B., Hatziioannou, T., McKeating, J.A., Bieniasz, P.D., Rice, C.M., 2007. Claudin-1 is a hepatitis C virus co-receptor required for a late step in entry. Nature 446 (7137), 801–805.

Flint, M., von Hahn, T., Zhang, J., Farquhar, M., Jones, C.T., Balfe, P., Rice, C.M., McKeating, J.A., 2006. Diverse CD81 proteins support hepatitis C virus infection. J. Virol. 80 (22), 11331–11342.

Fukuda, H., Terashima, M., Koshikawa, M., Kanegae, Y., Saito, I., 2006. Possible mechanism of adenovirus generation from a cloned viral genome tagged with nucleotides at its ends. Microbiol. Immunol. 50 (8), 643–654.

Han, Q., Xu, C., Wu, C., Zhu, W., Yang, R., Chen, X., 2009. Compensatory mutations in NS3 and NS5A proteins enhance the virus production capability of hepatitis C reporter virus. Virus Res. 145 (1), 63–73.

Helle, F., Vieyres, G., Elkrief, L., Popescu, C.I., Wychowski, C., Descamps, V., Castelain, S., Roingeard, P., Duverlie, G., Dubuisson, J., 2010. Role of N-linked glycans in the functions of hepatitis C virus envelope proteins incorporated into infectious virions. J. Virol. 84 (22), 11905–11915.

Hishiki, T., Shimizu, Y., Tobita, R., Sugiyama, K., Ogawa, K., Funami, K., Ohsaki, Y., Fujimoto, T., Takaku, H., Wakita, T., Baumert, T.F., Miyanari, Y., Shimotohno, K., 2010. Infectivity of hepatitis C virus is influenced by association with apolipoprotein E isoforms. J. Virol. 84 (22), 12048–12057.

Hoofnagle, J.H., 2002. Course and outcome of hepatitis C. Hepatology 36 (5 Suppl. 1), S21–9.

Hsu, M., Zhang, J., Flint, M., Logvinoff, C., Cheng-Mayer, C., Rice, C.M., McKeating, J.A., 2003. Hepatitis C virus glycoproteins mediate pH-dependent cell entry of pseudotyped retroviral particles. Proc. Natl. Acad. Sci. USA 100 (12), 7271–7276.

Ishii, K., Murakami, K., Hmwe, S.S., Zhang, B., Li, J., Shirakura, M., Morikawa, K., Suzuki, R., Miyamura, T., Wakita, T., Suzuki, T., 2008. Trans-encapsidation of hepatitis C virus subgenomic replicon RNA with viral structure proteins. Biochem. Biophys. Res. Commun. 371 (3), 446–450.

Jiang, J., Luo, G., 2009. Apolipoprotein E but not B is required for the formation of infectious hepatitis C virus particles. J. Virol. 83 (24), 12680–12691.

Jones, D.M., Atoom, A.M., Zhang, X., Kottilil, S., Russell, R.S., 2011. A genetic interaction between the core and NS3 proteins of hepatitis C virus is essential for production of infectious virus. J. Virol. 85 (23), 12351–12361.

Kanegae, Y., Lee, G., Sato, Y., Tanaka, M., Nakai, M., Sakaki, T., Sugano, S., Saito, I., 1995. Efficient gene activation in mammalian cells by using recombinant adenovirus expressing site-specific Cre recombinase. Nucl. Acids Res. 23 (19), 3816–3821.

Koch, J.O., Bartenschlager, R., 1999. Modulation of hepatitis C virus NS5A hyperphosphorylation by nonstructural proteins NS3, NS4A, and NS4B. J. Virol. 73 (9), 7138–7146.

Kummerer, B.M., Rice, C.M., 2002. Mutations in the yellow fever virus nonstructural protein NS2A selectively block production of infectious particles. J. Virol. 76 (10), 4773–4784.

Lavie, M., Goffard, A., Dubuisson, J., 2007. Assembly of a functional HCV glycoprotein heterodimer. Curr. Issues Mol. Biol. 9 (2), 71–86.

Lindenbach, B.D., Evans, M.J., Syder, A.J., Wolk, B., Tellinghuisen, T.L., Liu, C.C., Maruyama, T., Hynes, R.O., Burton, D.R., McKeating, J.A., Rice, C.M., 2005. Complete replication of hepatitis C virus in cell culture. Science 309 (5734), 623–626.

Liu, S., Yang, W., Shen, L., Turner, J.R., Coyne, C.B., Wang, T., 2009. Tight junction proteins claudin-1 and occludin control hepatitis C virus entry and are downregulated during infection to prevent superinfection. J. Virol. 83 (4), 2011–2014.

Liu, W.J., Sedlak, P.L., Kondratieva, N., Khromykh, A.A., 2002. Complementation analysis of the flavivirus Kunjin NS3 and NS5 proteins defines the minimal regions essential for formation of a replication complex and shows a requirement of NS3 in cis for virus assembly. J. Virol. 76 (21), 10766–10775.

Ma, Y., Yates, J., Liang, Y., Lemon, S.M., Yi, M., 2008. NS3 helicase domains involved in infectious intracellular hepatitis C virus particle assembly. J. Virol. 82 (15), 7624–7639.

Masaki, T., Suzuki, R., Saeed, M., Mori, K., Matsuda, M., Aizaki, H., Ishii, K., Maki, N., Miyamura, T., Matsuura, Y., Wakita, T., Suzuki, T., 2010. Production of infectious hepatitis C virus by using RNA polymerase I-mediated transcription. J. Virol. 84 (11), 5824–5835.

Mazumdar, B., Banerjee, A., Meyer, K., Ray, R., 2011. Hepatitis C virus E1 envelope glycoprotein interacts with apolipoproteins in facilitating entry into hepatocytes. Hepatology 54 (4), 1149–1156.

McKeating, J.A., Zhang, L.Q., Logvinoff, C., Flint, M., Zhang, J., Yu, J., Butera, D., Ho, D.D., Dustin, L.B., Rice, C.M., Balfe, P., 2004. Diverse hepatitis C virus glycoproteins mediate viral infection in a CD81-dependent manner. J. Virol. 78 (16), 8496–8505.

Owen, D.M., Huang, H., Ye, J., Gale Jr., M., 2009. Apolipoprotein E on hepatitis C virion facilitates infection through interaction with low-density lipoprotein receptor. Virology 394 (1), 99–108.

Please cite this article as: Suzuki, R., et al., *Trans*-complemented hepatitis C virus particles as a versatile tool for study of virus assembly and infection. Virology (2012), http://dx.doi.org/10.1016/j.virol.2012.05.033

ARTICLE IN PRESS

Pietschmann, T., Kaul, A., Koutsoudakis, G., Shavinskaya, A., Kallis, S., Steinmann, E., Abid, K., Negro, F., Dreux, M., Cosset, F.L., Bartenschlager, R., 2006. Construction and characterization of infectious intragenotypic and intergenotypic hepatitis C virus chimeras. Proc. Natl. Acad. Sci. USA 103 (19), 7408–7413.

Pileri, P., Uematsu, Y., Campagnoli, S., Galli, G., Falugi, F., Petracca, R., Weiner, A.J., Houghton, M., Rosa, D., Grandi, G., Abrignani, S., 1998. Binding of hepatitis C virus to CD81. Science 282 (5390), 938–941.

Ploss, A., Evans, M.J., Gaysinskaya, V.A., Panis, M., You, H., de Jong, Y.P., Rice, C.M., 2009. Human occludin is a hepatitis C virus entry factor required for infection of mouse cells. Nature 457 (7231), 882–886.

Russell, R.S., Meunier, J.C., Takikawa, S., Faulk, K., Engle, R.E., Bukh, J., Purcell, R.H., Emerson, S.U., 2008. Advantages of a single-cycle production assay to study cell culture-adaptive mutations of hepatitis C virus. Proc. Natl. Acad. Sci. USA 105 (11), 4370–4375.

Sainz Jr., B., Barretto, N., Martin, D.N., Hiraga, N., Imamura, M., Hussain, S., Marsh, K.A., Yu, X., Chayama, K., Alrefai, W.A., Uprichard, S.L., 2012. Identification of the Niemann-Pick C1-like 1 cholesterol absorption receptor as a new hepatitis C virus entry factor. Nat. Med. 18 (2), 281–285.

Sato, Y., Tanaka, K., Lee, G., Kanegae, Y., Sakai, Y., Kaneko, S., Nakabayashi, H., Tamaoki, T., Saito, I., 1998. Enhanced and specific gene expression via tissue-specific production of Cre recombinase using adenovirus vector. Biochem. Biophys. Res. Commun. 244 (2), 455–462.

Scarselli, E., Ansuini, H., Cerino, R., Roccasecca, R.M., Acali, S., Filocamo, G., Traboni, C., Nicosia, A., Cortese, R., Vitelli, A., 2002. The human scavenger receptor class B type I is a novel candidate receptor for the hepatitis C virus. EMBO J. 21 (19), 5017–5025.

Steinmann, E., Brohm, C., Kallis, S., Bartenschlager, R., Pietschmann, T., 2008. Efficient trans-encapsidation of hepatitis C virus RNAs into infectious virus-like particles. J. Virol. 82 (14), 7034–7046.

Suzuki, T., Ishii, K., Aizaki, H., Wakita, T., 2007. Hepatitis C viral life cycle. Adv. Drug Deliv. Rev. 59 (12), 1200–1212.

Tani, H., Komoda, Y., Matsuo, E., Suzuki, K., Hamamoto, I., Yamashita, T., Moriishi, K., Fujiyama, K., Kanto, T., Hayashi, N., Owsianka, A., Patel, A.H., Whitt, M.A., Matsuura, Y., 2007. Replication-competent recombinant vesicular stomatitis virus encoding hepatitis C virus envelope proteins. J. Virol. 81 (16), 8601–8612.

Vieyres, G., Thomas, X., Descamps, V., Duverlie, G., Patel, A.H., Dubuisson, J., 2010. Characterization of the envelope glycoproteins associated with infectious hepatitis C virus. J. Virol. 84 (19), 10159–10168.

Wakita, T., Pietschmann, T., Kato, T., Date, T., Miyamoto, M., Zhao, Z., Murthy, K., Habermann, A., Krausslich, H.G., Mizokami, M., Bartenschlager, R., Liang, T.J., 2005. Production of infectious hepatitis C virus in tissue culture from a cloned viral genome. Nat. Med. 11 (7), 791–796.

Yanagi, M., Purcell, R.H., Emerson, S.U., Bukh, J., 1997. Transcripts from a single full-length cDNA clone of hepatitis C virus are infectious when directly transfected into the liver of a chimpanzee. Proc. Natl. Acad. Sci. USA 94 (16), 8738–8743.

Zhong, J., Gastaminza, P., Cheng, G., Kapadia, S., Kato, T., Burton, D.R., Wieland, S.F., Uprichard, S.L., Wakita, T., Chisari, F.V., 2005. Robust hepatitis C virus infection in vitro. Proc. Natl. Acad. Sci. USA 102 (26), 9294–9299.

Please cite this article as: Suzuki, R., et al., *Trans*-complemented hepatitis C virus particles as a versatile tool for study of virus assembly and infection. Virology (2012), http://dx.doi.org/10.1016/j.virol.2012.05.033

Journal of Virology

Structural Basis for Broad Detection of Genogroup II Noroviruses by a Monoclonal Antibody That Binds to a Site Occluded in the Viral Particle

Grant S. Hansman, David W. Taylor, Jason S. McLellan, Thomas J. Smith, Ivelin Georgiev, Jeremy R. H. Tame, Sam-Yong Park, Makoto Yamazaki, Fumio Gondaira, Motohiro Miki, Kazuhiko Katayama, Kazuyoshi Murata and Peter D. Kwong

***J. Virol.* 2012, 86(7):3635. DOI: 10.1128/JVI.06868-11.**
Published Ahead of Print 25 January 2012.

Updated information and services can be found at:
http://jvi.asm.org/content/86/7/3635

These include:

SUPPLEMENTAL MATERIAL http://jvi.asm.org/content/suppl/2012/02/28/86.7.3635.DC1.html

REFERENCES This article cites 72 articles, 42 of which can be accessed free at: http://jvi.asm.org/content/86/7/3635#ref-list-1

CONTENT ALERTS Receive: RSS Feeds, eTOCs, free email alerts (when new articles cite this article), more»

Information about commercial reprint orders: **http://journals.asm.org/site/misc/reprints.xhtml**
To subscribe to to another ASM Journal go to: **http://journals.asm.org/site/subscriptions/**

Journals.ASM.org

Downloaded from http://jvi.asm.org/ on July 17, 2012 by NATL INST OF INFECTIOUS DISEAS

JVI
Journals.ASM.org

Structural Basis for Broad Detection of Genogroup II Noroviruses by a Monoclonal Antibody That Binds to a Site Occluded in the Viral Particle

Grant S. Hansman,[a,b] David W. Taylor,[c,d] Jason S. McLellan,[b] Thomas J. Smith,[e] Ivelin Georgiev,[b] Jeremy R. H. Tame,[f] Sam-Yong Park,[f] Makoto Yamazaki,[g] Fumio Gondaira,[g] Motohiro Miki,[a,g] Kazuhiko Katayama,[a] Kazuyoshi Murata,[d] and Peter D. Kwong[b]

Department of Virology II, National Institute of Infectious Diseases, Tokyo, Japan[a]; Vaccine Research Center, National Institute of Allergy and Infectious Diseases, National Institutes of Health, Bethesda, Maryland, USA[b]; Department of Molecular Biophysics and Biochemistry, Yale University School of Medicine, New Haven, Connecticut, USA[c]; National Institute for Physiological Sciences, Okazaki, Japan[d]; Donald Danforth Plant Science Center, Saint Louis, Missouri, USA[e]; Protein Design Laboratory, Yokohama City University, Yokohama, Japan[f]; and Denka-Seiken Co. Ltd., Niigata, Japan[g]

Human noroviruses are genetically and antigenically highly divergent. Monoclonal antibodies raised in mice against one kind of norovirus virus-like particle (VLP), however, were found to have broad recognition. In this study, we present the crystal structure of the antigen-binding fragment (Fab) for one of these broadly reactive monoclonal antibodies, 5B18, in complex with the capsid-protruding domain from a genogroup II genotype 10 (GII.10) norovirus at 3.3-Å resolution and, also, the cryo-electron microscopy structure of the GII.10 VLP at ~10-Å resolution. The GII.10 VLP structure was more similar in overall architecture to the GV.1 murine norovirus virion than to the prototype GI.1 human norovirus VLP, with the GII.10 protruding domain raised ~15 Å off the shell domain and rotated ~40° relative to the GI.1 protruding domain. In the crystal structure, the 5B18 Fab bound to a highly conserved region of the protruding domain. Based on the VLP structure, this region is involved in interactions with other regions of the capsid and is buried in the virus particle. Despite the occluded nature of the recognized epitope in the VLP structure, enzyme-linked immunosorbent assay (ELISA) binding suggested that the 5B18 antibody was able to capture intact VLPs. Together, the results provide evidence that the norovirus particle is capable of extreme conformational flexibility, which may allow for antibody recognition of conserved surfaces that would otherwise be buried on intact particles.

The family *Caliciviridae* contains four genera, *Norovirus*, *Sapovirus*, *Lagovirus*, and *Vesivirus*, which include norovirus, sapovirus, rabbit hemorrhagic disease virus, and feline calicivirus strains, respectively. Human noroviruses are the dominant cause of outbreaks of gastroenteritis and are genetically and antigenically distinct (21). Two main genogroups (GI and -II) of human noroviruses are mostly responsible for causing human infections, and these two genogroups are further subdivided into numerous genotypes (GI.1 to -8 and GII.1 to -17) (72). The human norovirus genome has three open reading frames (ORF1 to -3), where ORF1 encodes the nonstructural proteins, ORF2 encodes the capsid protein, and ORF3 encodes a small structural protein. Human noroviruses cannot be grown in cell culture, but the expression of the capsid protein in a baculovirus expression system leads to the self-assembly of nucleic acid-free virus-like particles (VLPs) that are believed to be morphologically and antigenically similar to the native virion (27).

The cryo-electron microscopy (cryo-EM) and X-ray crystal structures of the prototype norovirus VLP (GI.1, Norwalk virus) show that the VLP form a T=3 icosahedral structure (53, 54). The VLP can be divided into two domains, the shell (S) and the protruding (P) domains. The S domain forms a scaffold surrounding the RNA, whereas the P domain, which is further subdivided into P1 and P2 subdomains, is thought to contain the determinants of cell attachment and strain diversity (27, 53, 60). The P domain forms 90 dimer subunits, termed A/B and C/C. Interestingly, the P domains alone can be expressed in *Escherichia coli*, and these form P domain dimers that are biologically relevant (60). The X-ray crystal structures of several human norovirus P domains (GI.1, GII.4, GII.10, and GII.12) indicate that their overall structures are similar and resemble the P domain on the VLPs, with a single α-helix in the P1 subdomain and six antiparallel β-strands in the P2 subdomain (7, 10, 13, 22). The X-ray crystal structure of a GV.1 murine norovirus P domain reveals a structure that is similar overall to the human norovirus P domains (63). However, cryo-electron microscopy (cryo-EM) studies show that in the GV.1 murine norovirus virion, the P domain is raised off the S domain by ~16 Å (30), while in the GI.1 and GII.4 (Grimsby virus strain) human norovirus VLPs, the P domain rests directly on the S domain (12, 53, 54). In addition, the GV.1 murine norovirus P domain is rotated 40° clockwise with respect to the GI.1 and GII.4 human norovirus P domains.

Human noroviruses are generally detected using reverse transcription-PCR (RT-PCR) with degenerate primers or enzyme-linked immunosorbent assay (ELISA) with norovirus-specific antibodies. Many of the polyclonal and monoclonal antibodies (MAbs) used in the ELISA kits were developed in mice immunized with norovirus VLPs (15, 28, 55, 57), and most have broad recognition (21, 39, 40, 50, 59, 70). Several antibodies are found to bind to the S domain (39, 70), while others bound to the P domain (50, 59). However,

Received 23 November 2011 **Accepted** 10 January 2012
Published ahead of print 25 January 2012
Address correspondence to Peter D. Kwong, pdkwong@nih.gov, or Kazuyoshi Murata, kazum@nips.ac.jp.
Supplemental material for this article may be found at http://jvi.asm.org/.
Copyright © 2012, American Society for Microbiology. All Rights Reserved.
doi:10.1128/JVI.06868-11

Downloaded from http://jvi.asm.org/ on July 17, 2012 by NATL INST OF INFECTIOUS DISEAS

structural details of the antibody mode of binding to the VLPs, S domain or P domain, have been lacking. In the studies presented here, we used X-ray crystallography to define the recognition site of the broadly reactive antibody 5B18 on the norovirus GII.10 P domain, cryo-EM to determine the structure of the intact GII.10 VLP, and ELISA to determine whether this antibody recognizes intact or disassembled virus particles. Overall, the findings have implications related to the dynamic nature of the P domain in the context of the norovirus VLP and to its recognition by antibody.

MATERIALS AND METHODS

Norovirus VLP expression. The GII.4 Saga (GenBank accession number BAG70515), GII.10 Vietnam026 (GenBank accession number AF504671) (23), and GII.12 Hiro (GenBank accession number AB044366) (23) VLPs were expressed as previously described (23). The VLPs were purified using CsCl equilibrium gradient ultracentrifugation at 35,000 rpm for 24 h at 4°C (Beckman SW55 rotor). A distinct viral band was removed from the side of the tube with a syringe and the VLPs were stored in phosphate-buffered saline (PBS) (pH 7.3) at 4°C. The integrity of the VLPs was confirmed by negative-stain EM. Briefly, the VLP samples were applied to a carbon-coated 300-mesh EM grid and stained with 2% uranyl acetate (pH 4). Grids were examined using a Jeol JEM-1220 transmission electron microscope operated at 80 kV.

Antibody ELISA binding to GII.4, GII.10, and GII.12 VLPs. An antibody ELISA was used to compare the cross-reactivities of VLPs from the three different GII norovirus genotypes (GII.4, GII.10, and GII.12) with 5B18 IgG. Wells of 96-well microtiter plates (MaxiSorp; Nunc, Denmark) were each coated with 100 μl of ~100 ng of purified VLPs (in PBS, pH 7.3) and incubated overnight at 4°C. The wells were washed four times with PBS containing 0.1% (vol/vol) Tween 20 (PBS-T) and then were blocked with PBS containing 5% (wt/vol) skim milk for 1 h at room temperature. After the wells were washed four times with PBS-T, 100 μl of 2-fold serially diluted horseradish peroxidase (HRP)-conjugated labeled 5B18 IgG, from a 1:5,000 starting dilution in PBS containing 0.05% (wt/vol) skim milk, was added to each well, and the plates were incubated for 1 h at 37°C. The wells were washed four times with PBS-T, and then 100 μl of 3,3′,5,5′-tetramethylbenzidine substrate was added to each well. The reaction was stopped by the addition of 100 μl of 2 N H_2SO_4 to each well, and the absorbance was measured at 450 nm (A_{450}). The titer was expressed as the reciprocal of the highest dilution of antiserum giving a value of A_{450} of >0.2, as previously described (21).

Western blotting. The VLPs and P domains were separated by SDS-PAGE and electrotransferred to polyvinylidene difluoride (PVDF) membranes by using iBLOT, following the manufacturer's protocol. Proteins were detected with 5B18 IgG at a dilution of 1:5,000, and then, following the manufacturer's instructions, the blots were developed by chemiluminescence using enhanced chemiluminescence (ECL) detection reagent (Amersham Biosciences, England).

Protein expression and purification of GII.10 P domain. The GII.10 P domain was expressed in *E. coli* and purified as previously described (22). Briefly, the P domain was optimized for *E. coli* expression, cloned in a modified pMal-c2x vector at the BamHI and NotI restriction sites (New England BioLabs), and transformed into BL21(DE3) cells (Invitrogen). Expression was induced with IPTG (isopropyl-β-D-thiogalactopyranoside) (1 mM) for 18 h at 22°C. After a series of purification steps and protease cleavage, the P domain was concentrated to 2 to 10 mg/ml and stored in gel filtration buffer (0.35 M NaCl, 2.5 mM Tris, pH 7.0, 0.02% NaN_3).

Preparation of 5B18 Fab fragment. The 5B18 IgG monoclonal antibody was produced from a mouse immunized with GII.4 norovirus-445 VLPs (GenBank accession number DQ093064) (Denkaseiken, Japan). The 5B18 IgG is currently used as a GII broad-range capture antibody in a commercially available ELISA kit (Denkaseiken, Japan). The 5B18 Fab was prepared using a modified method (34). Approximately 60 mg of purified 5B18 IgG was used for Fab preparation. IgG was reduced in 100 mM dithiothreitol (DTT) (pH 7.6) for 1 h at 37°C. The reduced IgG was added to a dialysis cassette, and the DTT was removed by placing the cassette in GFB (0.35 M NaCl, 2.5 mM Tris, pH 7.0, 0.02% NaN_3) supplemented with 20 mM HEPES (pH 7.7) for 1 h at 4°C. The IgG was alkylated in the same buffer supplemented with 2 mM iodoacetamide for 48 h at 4°C, and then the cassette was transferred to a fresh solution without the iodoacetamide for 1 h at 4°C. The IgG was concentrated to 5 mg/ml and then digested with papain using a commercial kit (Pierce, Rockford, United States). The Fab was separated from the Fc in a protein A column, and the resulting Fab was further purified by size exclusion chromatography with a Superdex 200 column (GE), concentrated to 5 mg/ml, and stored in GFB. The purified GII.10 P domain and Fab were mixed 1.4:1 for 1 h at 25°C, and finally, the GII.10 P domain-Fab complex was purified by size exclusion chromatography.

Preparation and cocrystallization of GII.10 P domain-Fab complex for X-ray crystallography. Crystals of the GII.10 P domain-Fab complex were grown by the hanging drop vapor diffusion method, mixing the protein and reservoir solution (40% [vol/vol] polyethylene glycol [PEG] 400, 5% [wt/vol] PEG 3350, and 0.1 M acetic acid, pH 5.5) (42) in a 1:1 ratio. Crystals grew over 1 week at a temperature of 20°C. Prior to data collection, crystals were transferred to 50% (vol/vol) PEG 400.

X-ray crystallography data collection, structure solution, and refinement. X-ray diffraction data were collected at the Southeast Regional Collaborative Access Team (SER-CAT) beamline 22-BM at the Advanced Photon Source, Argonne National Laboratory, Argonne, IL, and processed with HKL2000 (49). Despite the large size of the crystals (perfectly formed pyramids of up to 0.3 mm per edge), the diffraction data were poor due to split reflections, high background, and most diffraction extending to less than 4 Å. These resulted in Chi^2 values of 0 for several wedges of data. Despite these difficulties, relatively complete data (90%) was obtained from 180 degrees of oscillation, though with lower than expected redundancy (2.7-fold), and the overall quality of data which passed the Chi^2 tests appeared fine. Structures were solved by molecular replacement in PHASER (44), using the structure with Protein Data Bank identifier (PDB ID) 3ONU for the GII.10 P domain and the structure with PDB ID 1WEJ for the Fab as a search model. Manual model building was performed in COOT (18), and positional refinement together with translation/liberation/screw (TLS) refinement were performed using REFMAC (14) and PHENIX (1).

Cryo-EM data collection and refinement. VLPs at a concentration of 1.0 mg/ml were applied to a glow-discharged Quantifoil R1.2/1.3 Mo 200-mesh holey carbon grid with a thin layer of carbon over the holes. The sample was rapidly plunged into liquid ethane after automatic blotting for 7 to 8 s at 8°C and 100% humidity using an FEI MarkIV Vitrobot. Grids were examined with a JEOL JEM-2200FFC microscope equipped with a field emission gun and an in-column (omega-type) energy filter operated at an acceleration voltage of 200 kV. Images of the frozen VLPs were collected at a nominal magnification of 40,000 using a 4k × 4k (4,096- by 4,096-pixel) Tietz charge-coupled-device (CCD) camera, resulting in a pixel size of 2.4 Å. Particles were extracted from raw micrographs using the swarm semiautomatic particle-picking algorithm in EMAN2 into boxes of 250 by 250 square pixels (61). The raw particles were normalized, phase flipped, and high-pass filtered before single-particle analysis. Approximately 8,000 particle images were subjected to two-dimensional (2-D) reference-free alignment and classification through several rounds of multireference alignment and multivariate statistical analysis in IMAGIC to a total of 50 classes (65). Approximately 80% of the data were used for the reconstruction. Particles with cross-correlation values 1.5 σ below the mean were not used (~20%). Representative class averages were used as the basis for initial model generation in EMAN2. The initial model with the best match between reprojections and class averages was chosen as the starting model for several rounds of projection-matching refinement with increasing angular sampling. The final reconstruction, at ~10-Å resolution (0.5 Fourier shell correlation [FSC] criterion), was used for atomic coordinate fitting and structure comparison in Chimera (version 1.5.3) (52).

Downloaded from http://jvi.asm.org/ on July 17, 2012 by NATL INST OF INFECTIOUS DISEAS

Structure analysis, sequence analysis, and figures. Figures were rendered using PyMOL (version 1.2r3; Schroedinger LLC) and Chimera (version 1.5.3) (52). The N-terminal amino acid sequences for the Fab heavy and kappa (κ) chains were determined at the Columbia University Medical Center, Protein Core Facility. Degenerate primers for the Fab sequence were designed from constant regions and from the N-terminal amino acid sequence based on closely matching murine antibody N-terminal nucleotide sequences in GenBank. Norovirus complete-capsid amino acid sequences were aligned and analyzed with GenetyxMac software (version 16.0.0).

Antibody ELISA binding to GII.10 VLPs at different pHs. An antibody ELISA was used to determine the ability of 5B18 IgG to bind to GII.10 VLPs. The GII.10 VLPs were diluted in PBS at pHs 5.3, 6.3, 7.3, 8.3, and 9.3 to a final concentration of 7.5 μg/ml. At high PBS pHs, the VLPs were found to be partially broken, while at low pHs, most of the VLPs were intact. Wells of 96-well microtiter plates (MaxiSorp; Nunc, Denmark) were each coated with 100 μl of 7.5 μg/ml of VLPs at the different pHs and incubated overnight at 4°C. The VLPs were detected as described above, except that 5B18 IgG and goat HRP–anti-mouse IgG (used as a secondary antibody) replaced the HRP-labeled 5B18 IgG. After the addition of the secondary antibody, the wells were washed four times with PBS-T, and then 100 μl of substrate *o*-phenylenediamine and H_2O_2 was added to each well and the plates left in the dark for 30 min at room temperature. The reaction was stopped by the addition of 50 μl of 2 N H_2SO_4 to each well, and the absorbance was measured at 492 nm (A_{492}).

Sequence conservation on the VLP and P domain. To show the sequence conservation on the GII VLP, a model of the GII.10 VLP was built as described previously (22) using the unbound GII.10 P domain structure (PDB ID 3ONU) and the S domain from the Norwalk virus capsid structure (PDB ID 1IHM). Amino acid sequence conservation was analyzed as previously described (22). Briefly, an alignment of a representative set of GII sequences was used to compute residue conservation scores using the AL2CO server (51) and mapped (using a color range for highly variable to highly conserved residues) onto the surface of the GII.10 VLP model and unbound GII.10 P domain structure.

Accession numbers. Atomic coordinate and structure factors of the X-ray crystal structure were deposited in the Protein Data Bank under accession number 3V7A. The 3-D cryo-EM map was deposited in the EMDataBank with accession number EMD-5374.

RESULTS

5B18 binds to several GII genotypes. To confirm the ability of the 5B18 IgG to bind diverse GII norovirus genotypes, we expressed VLPs from three GII genotypes (GII.4, GII.10, and GII.12) and examined the binding using ELISA and Western blotting. The EM results showed that GII.4 VLPs were a mixture of small and native-size particles, while the GII.10 and GII.12 VLPs were mostly of native size (data not shown). The ELISA results showed that 5B18 IgG was capable of cross-reacting with all three GII genotypes having an equal titer of 320,000 (see Fig. S1A in the supplemental material). The Western blotting results also showed that the 5B18 IgG could detect the three GII genotypes (see Fig. S1B).

X-ray crystal structure of GII.10 P domain-Fab complex. The GII.10 P domain was used to determine the precise binding location of the 5B18 antibody on the norovirus capsid using X-ray crystallography. The GII.10 P domain and Fab proteins were mixed together (1.4:1 molar ratio) for 1 h at room temperature. The GII.10 P domain-Fab complex was purified using size exclusion chromatography. Two main peaks were observed, corresponding to the complex and free P domain (data not shown). The fractions containing the GII.10 P domain-Fab complex were pooled and concentrated to ~4 mg/ml, and the complex was crystallized by the hanging-drop vapor diffusion method. A single GII.10 P domain-Fab complex crystal diffracted X rays to ~3.3 Å. The structure was solved using molecular replacement with a GII.10 P domain monomer (PDB ID 3ONU) and a mouse Fab (PDB ID 1WEJ) as search models. Molecular replacement indicated that two P domain monomers and two 5B18 Fabs each containing a kappa (κ) chain and heavy chain were in the asymmetrical unit and these were related by a noncrystallographic 2-fold. Water molecules were not added to the structure since the resolution was at 3.3 Å. The 5B18 Fab was shown to bind to the wall of the P1 subdomain and involved a monomeric interaction with the P1 subdomain (Fig. 1A). The electron densities of the P domains and 5B18 Fabs were generally well defined, and refinement led to an R_{value} of 0.230 (R_{free} of 0.283) (Table 1; also see Fig. S2 in the supplemental material). The P domain dimer had a single helix in each P1 subdomain and six antiparallel β-strands in each P2 subdomain as previously described (22).

GII.10 P domain interaction with the 5B18 Fab. The total interface area of the GII.10 P domain and 5B18 Fab was 1,500 Å^2 (770 Å^2 on the P domain and 730 Å^2 on the 5B18 Fab), as calculated using PISA software (33). The GII.10 P domain and 5B18 Fab interaction included nine hydrogen bonds, eight of which were formed between the P1 subdomain and κ chain and one between the P1 subdomain and heavy chain (Fig. 1B; also see Table S1 in the supplemental material). Six P1 subdomain amino acids interacted with the 5B18 Fab, Tyr533 formed a single hydrogen bond with Tyr92κ, Thr534 formed three hydrogen bonds with Gly93κ and one hydrogen bond with Trp97κ, Leu535 formed a hydrogen bond with Tyr32κ, Glu496 formed a hydrogen bond with Tyr92κ, Asn530 formed a hydrogen bond with Ser94κ, and Val433 formed a hydrogen bond with Asn52 heavy chain. Superposition of the apo GII.10 P domain dimer and the Fab-bound GII.10 P domain showed that each of the P1 subdomains shifted slightly (~1 to 2 Å) toward the center of the dimer, while the P2 subdomain showed little conformational change (see Fig. S3 in the supplemental material). The electrostatic potential of the Fab was calculated (16), and the interacting residues on the P domain bound at two negatively charged pockets on the Fab at the variable regions (Fig. 2).

Conservation of the 5B18 Fab-binding site on GII P domains. The 5B18 Fab formed hydrogen bonds with residues at three different sites on the P1 subdomain, termed A, B, and C (Fig. 3). An amino acid alignment of representatives from 10 GII norovirus genotypes indicated that Val433 (site A) was the most variable, with other genotypes having threonine, serine, asparagine, leucine, or methionine at this position. Thr534 (site C) was mostly conserved, as the only other amino acid at this position was a serine. Glu496 (site B), Asn530 (site C), Tyr533 (site C), and Leu535 (site C) were all highly conserved among the representative GII genotypes. Superposition of other known GII norovirus P domains (GV.1, GII.4-TCH05, GII.4-VA387, GII.12, GII.9-VA207, and GI.1) showed that the equivalent GII.10 interacting side chains were mostly in the same conformation (see Fig. S4 in the supplemental material). GI norovirus side chains also appeared to be similar to the GII.10 interacting side chains (see Fig. S4).

GII.10 VLP cryo-EM structure. From the general location of the epitope (Fig. 1) and the known structures of other caliciviruses (7, 10, 13, 22), it was not clear how the monoclonal antibody, raised against intact VLPs, could bind at this occluded site on intact particles. To this end, the cryo-EM structure of the GII.10 VLP (in an unbound state) was determined to define the arrange-

Downloaded from http://jvi.asm.org/ on July 17, 2012 by NATL INST OF INFECTIOUS DISEAS

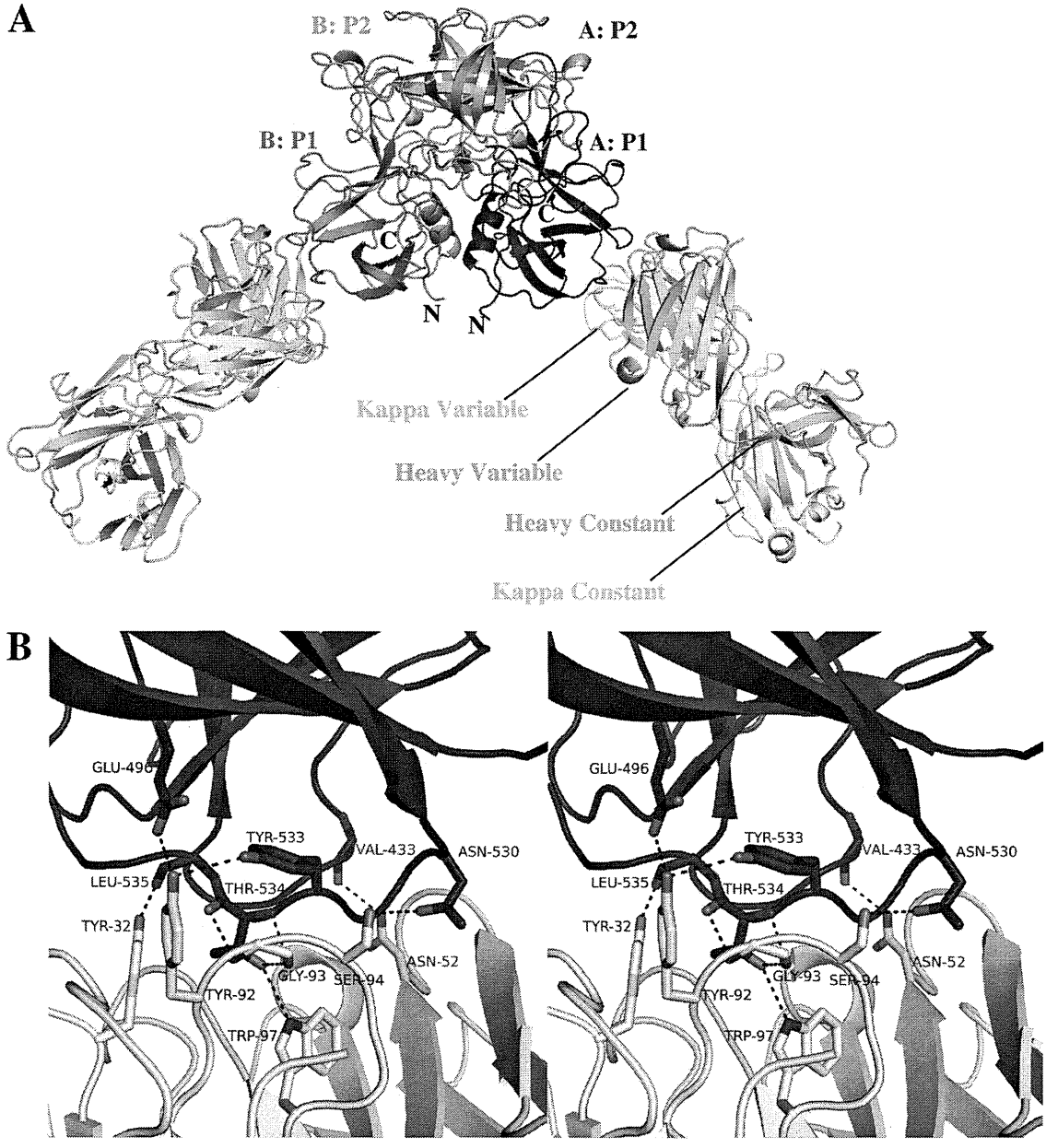

FIG 1 The X-ray crystal structure of the GII.10 P domain-Fab complex shows that the Fab bound to the lower side of the P1 subdomain. The GII.10 P domain dimer is colored according to monomers and subdomains, i.e., chain A: P1 (blue), chain A: P2 (light blue), chain B: P1 (violet), and chain B: P2 (salmon), whereas the Fab is colored according to chain, i.e., κ chain (yellow) and heavy chain (green). (A) The Fab bound to the wall of the P1 subdomain (considered to be inside the virus particle) and involved a monomeric interaction. (B) A close-up stereoview of the interacting P domain residues for chain A (Val433, Glu496, Asn530, Tyr533, Thr534, and Leu535) and Fab residues (κ chain, Tyr32, Tyr92, Gly93, Ser94, and Trp97, and heavy chain, Asn52). The hydrogen bond interactions included both side chain and main chain interactions (also see Table S1 in the supplemental material).

ment of the GII.10 P domains with respect to the entire capsid. The GII.10 VLPs appeared as homogeneous, monodisperse particles in ice (see Fig. S5A in the supplemental material). Reference-free class averages of the VLPs showed icosahedral particles with spike-like structures extending from the vertices (see Fig. S5). The cryo-EM reconstruction of the GII.10 VLP at ~10-Å resolution (0.5 FSC criterion) showed several striking features (Fig. 4). The GII.10 S domain was noticeably surface exposed at the 3- and 5-fold axes (Fig. 4A). The GII.10 P domain appeared as a second outer shell, and a central section through the VLP revealed that the P domain was raised off the S domain by ~15 Å (Fig. 4B). The electron density at the tip of the P domain (the P2 subdomain) was significantly weaker than at the base of the P1 domain, suggesting that there was marked flexibility in the P2 subdomains. This was consistent with what has been observed with several other reconstructions of calicivirus particles (4, 5) and suggests that there is a great deal of conformational heterogeneity in the P domains.

Fitting of the GII.10 P domain and P domain-Fab complex into the GII.10 VLP cryo-EM structure. At ~10-Å resolution, the GII.10 P domain monomers on the VLP were easily distinguished.

Downloaded from http://jvi.asm.org/ on July 17, 2012 by NATL INST OF INFECTIOUS DISEAS

TABLE 1 Data collection and refinement statistics for the GII.10 norovirus P domain-Fab complex structure

Parameter	Value[a]
Data collection	
Space group	$P\,4_322$
Cell dimensions	
a, *b*, *c* (Å)	145.48, 145.48, 216.33
α, β, γ (°)	90, 90, 90
Resolution (Å)	50-3.30 (3.42-3.30)[b]
R_{sym}	15.0 (55.1)
$I/\sigma I$	8.3 (1.8)
Completeness (%)	87.6 (89.0)
Redundancy	2.7 (2.7)
No. of unique reflections	31,300
Refinement	
Resolution (Å)	31.54–3.30
No. of reflections	30,833
R_{work}/R_{free}	0.227/0.283
No. of atoms	11,459
Average *B* factors (Å^2)	
Overall	84.7
P domain	82.4
Fab	86.3
Ramachandran (%)	
Outliers	0.00
Favored	93.31
RMS deviations	
Bond lengths (Å)	0.004
Bond angles (°)	0.795

[a] The data set was collected from a single crystal of the 026_P domain-Fab complex (PDB ID 3V7A).
[b] Values in parentheses are for the highest-resolution shell.

Fitting of the crystal structures of the GII.10 P domain and P domain-Fab complex into the GII.10 VLP cryo-EM map was performed manually and guided by previous fitting results of GV.1 P domain dimers into the GV.1 cryo-EM map (63). This approximate alignment was adjusted computationally using the Fit-in-Map function in UCSF Chimera (52) to a cross-correlation coefficient of 0.94 (Fig. 4). Using this method, the X-ray structure of the GII.10 P domain dimer (PDB ID 3ONU) was unambiguously fitted into the corresponding density in the cryo-EM map, except for several loops on the P2 subdomain (Fig. 4C). This is probably due to flexibility in these domains, as the electron density of the P2 subdomain loops was weak and the tips of the P2 domains were less ordered than the S domain and P1 domains in the cryo-EM reconstruction (data not shown). The P domain dimers appeared to be connected to adjacent, icosahedrally related P1 subdomains in the VLP, whereas the P2 subdomains had no such connections (Fig. 4C). When the P domain from the X-ray structure of the P domain-Fab complex was fitted into the A/B dimer subunit of the reconstruction, the 5B18 Fab was located under the neighboring P domain dimer and rested on top of the S domain at the space at the 2-fold axes (Fig. 5A). When the P domain from the X-ray structure of the P domain-Fab complex was instead fitted into the C/C dimer subunit, the 5B18 Fab made contact with a neighboring P domain dimer and clashed with a star-like protrusion on the S domain at the space at the 5-fold axes (Fig. 5B). Essentially, the epitope of 5B18 overlapped the region of the P1 subdomain that made interactions with icosahedrally related, adjacent P domains in the VLPs when in this "floating P domain" conformation. Based on this modeling, it appeared that the VLP probably could not be saturated with 5B18 antibodies, as this would create a highly unstable structure, as well as additional IgG-IgG steric clashes at the axis spaces. Two possibilities are likely, (i) that 5B18 recognition of intact norovirus particles occurs at select, transiently exposed P domains or (ii) that 5B18 recognition occurs at places where the particle has a defect, where the P domain is exposed because the particle is not appropriately formed.

The 5B18 IgG bound equally well with intact and partially broken GII.10 VLPs. To test whether 5B18 recognition occurs with intact or with broken particles, we assessed the pH behavior of 5B18 recognition, as norovirus VLPs become less stable and appear broken at high pH values (2). We observed that at low and neutral pHs (5.3, 6.3, and 7.3), the GII.10 VLPs were mostly homogenous in size and unbroken, whereas at higher pHs (8.3 and 9.3), the GII.10 VLPs appeared less homogenous in size and partially broken (Fig. 6A). The 5B18 IgG detected GII.10 VLPs at different pH values with nearly identical efficacy, regardless of the fraction of damaged particles (Fig. 6B). At pH 5.3, 6.3, and 8.3, the titer was 512,000, at pH 9.3, the titer was 1,024,000, and at pH 7.3, the titer was 2,048,000 (optical density [OD] cutoff of >0.2) (21).

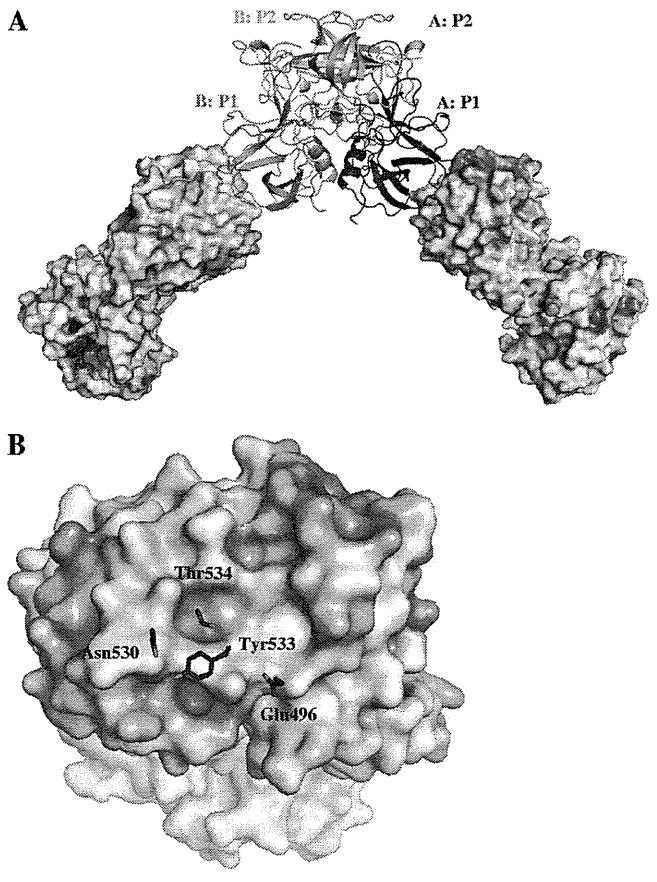

FIG 2 The binding site on the Fab was coordinated by negative charge regions on the Fab. (A) The GII.10 P domain is colored as in Fig. 1. The 5B18 Fab surface is color-coded according to electrostatic potential from red (negative charge) to blue (positive charge). (B) A close-up view of the electrostatic potential on the Fab, showing the four P domain side chain residues on chain A that interacted with the Fab. The P domain side chains bound near the negative charge (red) regions on the Fab.

Downloaded from http://jvi.asm.org/ on July 17, 2012 by NATL INST OF INFECTIOUS DISEAS